**Title**
Modulating Hot Electron Transfer between Plasmonic Nanostructures and 2D Semiconductors



**Author**
Feng, Ziying

**Publication Date**
2020

Peer reviewed|Thesis/dissertation

UNIVERSITY OF CALIFORNIA

Los Angeles

# Modulating Hot Electron Transfer between Plasmonic Nanostructures and 2D Semiconductors

A dissertation submitted in partial satisfaction of the

requirements for the degree Doctor of Philosophy

in Chemistry

by

Ziying Feng

2020

ABSTRACT OF THE DISSERTATION

Modulating Hot Electron Transfer between Plasmonic Nanostructures and 2D Semiconductors

by

Ziying Feng

Doctor of Philosophy in Chemistry

University of California, Los Angeles, 2020

Professor Xiangfeng Duan, Chair

Plasmonic hot electrons are electrons with high kinetic energy, generated from the plasmonic nanostructures. The application of hot electrons has been widely studied in the community of photochemistry and optoelectronics. Many applications like photoelectrochemistry and photodetector involve semiconductors, and these applications are plagued by low hot electron injection efficiency in the metal-semiconductor junctions which hinders the wider applications for the hot electrons.

Since the exfoliation of graphene with scotch tape in 2004, two dimensional (2D) materials have been widely studied for their unique properties when the thickness scales down to atomically thin. Transition metal dichalcogenides are a class 2D materials, they are semiconductors, and they have the different band structures with different material compositions. For each type of the transition metal dichalcogenide, its few-layer counterparts have both direct band transition and the indirect band transition, this unique band structure of the few-layer 2D transition metal dichalcogenides opens up the possibilities for studying the relationship between the hot electron injection and the band structure in the metal-semiconductor junction.

Inspired by the unique band structure of the 2D semiconductors, we design the structure formed with plasmonic nanostructures and 2D semiconductors as a model system to explore plasmonic hot electron injection process at the metal-semiconductor junction, in which we employ high mobility 2D semiconductor to capture the hot electrons. Due to the high photoluminescence quantum yield $WSe_2$, photoluminescence spectra are sued to probe the hot electron injection mechanism between the gold and few-layer $WSe_2$. We demonstrated that the hot electrons tend to at first inject into the energy lower $\Lambda$ point, and then to the $K$ point of the of the few-layer $WSe_2$.

Another question considered in this dissertation is how to modulate the hot electron injection to improve hot electron collection in the semiconductor. We employed self-assembled monolayer alkane thiols with different chain lengths as the interlayer, and polymethyl methacrylate (PMMA) as protection layer to tune hot electron transfer process. The insight derived provides valuable guidance for the rational design and performance optimization of the relevant plasmonic hot electron devices.

This dissertation of Ziying Feng is approved.

Stuart Brown

William M. Gelbart

Xiangfeng Duan, Committee Chair

University of California, Los Angeles

2020

*Dedicated to my parents and grandparents*

*for their love and unconditional support.*

# TABLE OF CONTENTS

# LIST OF FIGURES

ACKNOWLEDGMENTS

First and foremost, I would like to use this opportunity to express my sincere gratitude to my advisor Professor Xiangfeng Duan for their patient guidance, mentorship and inspiration throughout my entire PhD study and research. Professor Duan gave me an opportunity to join his group in September 2014, and since then he has helped shaped me into a passionate independent researcher by discussing with me and sharing with me insights and experience to help me through my projects. He also encouraged me to take challenge and devise novel ideas, and he also gave me a lot of support and guidance on my ideas. He spent a lot of time looking at my results and discussed with me in detail about the edge cases and corner cases of my projects. His dedication and attitude towards research set a role model for me.

I would like to thank Professor Stuart Brown and Professor William M. Gelbart to be my committee members. I would also like to thank Professor Kendall N. Houk for discussion of my qualifying exam and my fourth-year meeting. They spent their precious time giving me valuable suggestions and helpful insights. I would also like to thank Professor Yu Huang from the MSE department for useful discussions about my projects.

I would like to extend my thanks to all the labmates from the chemistry department and the MSE department. First of all, I would like to thank Dr. Chuancheng Jia, he was my mentor and guided me though the door of hot electron. Secondly, I would like to thank Dr. Yuan Liu, he introduced me to the device fabrication skills and device physics. Third, I would like to thank Dr. Zheng Fan and Dr. Zipeng Zhao who taught me knowledge about the electrochemistry and characterization.

Finally, I would like to express my gratitude to my parents and brother, for their continued support and encouragement for the pursuit of the Ph.D. degree.

# VITA

| | |
|---|---|
| 2014 – present | Ph.D. Student, Chemistry<br>University of California, Los Angeles<br>Los Angeles, CA, United States |
| 2010 – 2014 | B.S., Optic Informatics<br>Sun Yat-Sen University<br>Guangzhou, China |

## Chapter 1 : Plasmonic Hot Electron

### 1.1 Hot Electron and Photoelectrochemistry

Plasmonic is the phenomenon of the collective oscillation charge carriers at the surface metal, and these electrons are called surface plasmon (Figure 1.1). [1] When the surface plasmon dephases through the interband or intraband transition, hot electrons with high kinetic energy will be generated. In the typical plasmonic metals (normally noble metals such as gold and silver), the electronic band structure includes two types of bands, the sp-band and the d-bands. Therefore, light illumination generates two types of excited carriers, promoted through intraband and interband transitions. [2] The hot electrons in this dissertation refer to the intraband transitions, we focus on the intraband transition because they are able to generate excited electrons with high energy above the Fermi level, which means the electrons are "hot".[2] "Hot" means the effective temperature used to model carrier density. The property of plasmonic effect is that the electricmagnetic field can be enhanced by orders of magnitude,[3] which provides the electrons with kinetic energy.

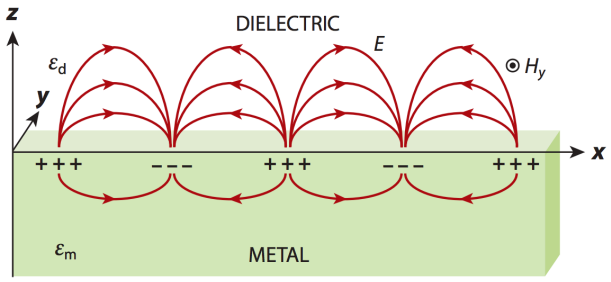


**Figure 1.1** Schematic illustration of surface plasmon. [1] Image adapted from Ref. 1.

Because of the "hot" property of the plasmonic generated hot electrons, they have attracted increasing attention to improve the harvest of efficiency of photovoltaic, photodetector and photoelectrochemistry reaction (Figure 1.2).[6-15, 20] There are Thomas White *et al.* provides calculation for theoretical IPEC (incident photon-to-current conversion efficiencies) of the metal-

semiconductor system and the calculation shows that the IPEC would reach up to 22.6%.[17] Tetsu Tatsuma *et al.* investigated the gold nanoparticle nanoporous $TiO_2$ composites (Au-$TiO_2$) and demonstrated that the system could be used as photocatalysts that oxidizes ethanol and methanol and reduces oxygen.[16] Martin Moskovits *et al.* designed an autonomous photosynthesis device using gold nanorod and $TiO_2$ with the Pt as the reduction catalyst and cobalt-based oxygen evolution catalyst.[20] Suljo Linic *et al.* studied the silver nanostructure as catalysts for oxidation reactions such as ethylene epoxidation, CO oxidation and $NH_3$ oxidation, the results demonstrate that with the plasmonic effect the catalysts could be able to drive the reactions at a 25 K lower temperature, which would increase the lifetime of the catalysts lifetime 10 folds compared to that using only the thermal process to drive the reactions.[18] Naomi Halas *et al.* reported an active optical antenna device for the detection of light, due to its integration with silicon this photodetector advantaged over the costly InGaAs detectors.[19]

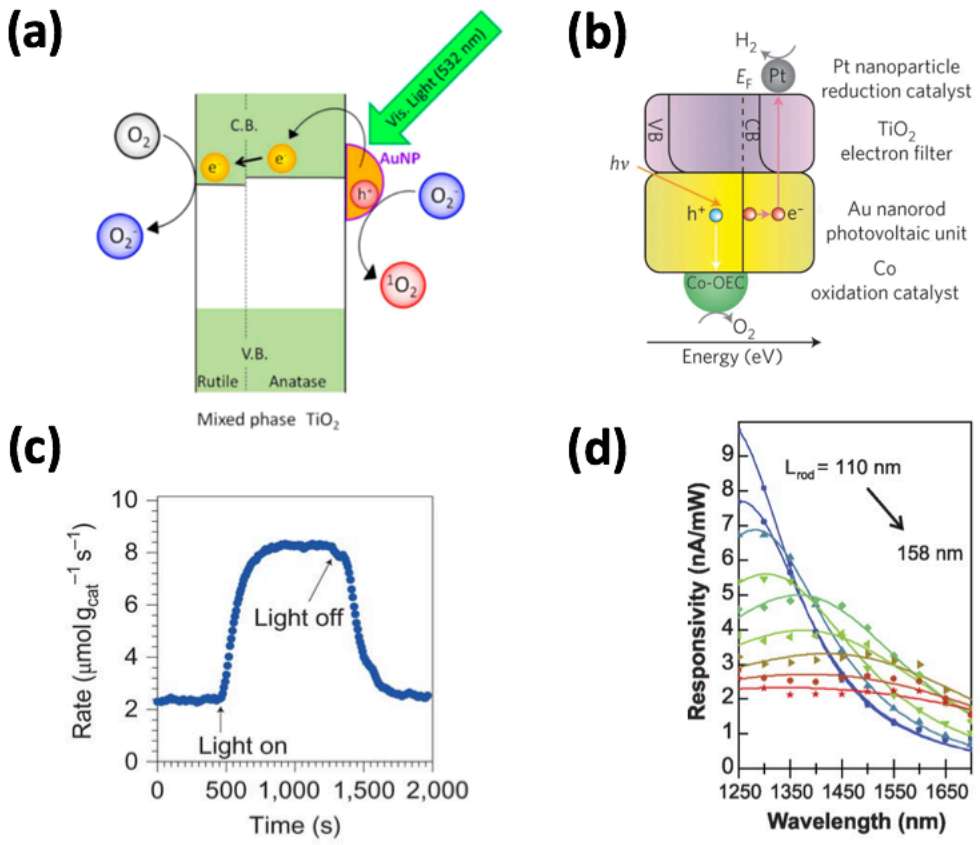


**Figure 1.2** Plasmonic hot electron applications. (a) Au-$TiO_2$ system used as photocatalysts that reduces oxygen. [16] Adapted with permission from Ref. 16 Copyright © 2005, American Chemical Society. (b) Autonomous photosynthesis device using gold nanorod and $TiO_2$ with the Pt as the reduction catalyst and cobalt-based oxygen evolution catalyst. [19] From Ref. 19 Copyright © 2013, Springer Nature. (c) Plasmonic silver nanostructure enhanced oxidation reaction. [18] From Ref. 18 Copyright © 2011, Springer Nature. (d) Plasmonic photodetector. [14] From Ref. 14. Reprinted with permission from AAAS.

Wei David Wei *et al.* have summarized the plasmonic hot electron transfer pathways and time scales (Figure 1.3). Amongst all the transfer pathways, we are most interested in those in the presence of adsorbate and in the presence of semiconductor, because we the purpose of this

dissertation is to study the electron transfer process so as to improve the application of hot electrons, and the application of hot electrons are associated with being in contact with either adsorbates or semiconductors. When impregnate the plasmonic structure onto the semiconductor, the hot electrons will transfer to the conduction band of the semiconductor due to the high kinetic energy.

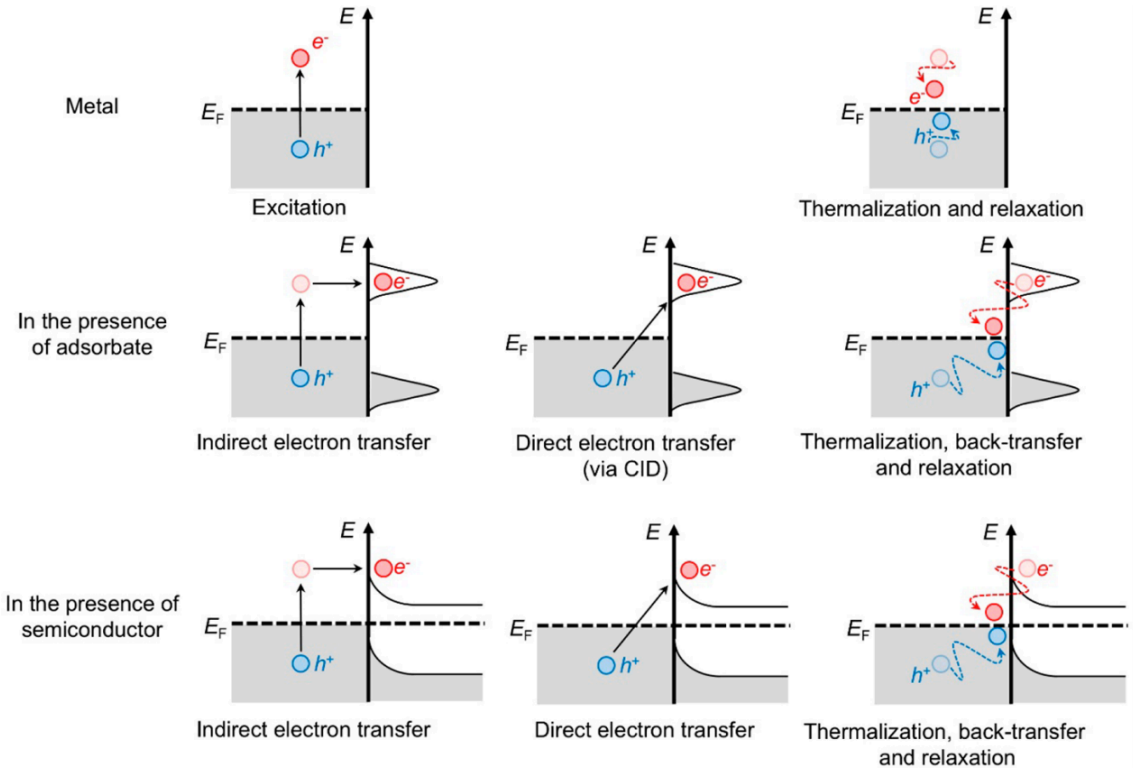


**Figure 1.3** Plasmon-induced hot carrier generation and hot electron transfer / back-transfer processes in clean metal, metal / adsorbate, and metal / semiconductor systems.[2] Adapted with permission from Ref. 2 Copyright © 2017, American Chemical Society.

### 1.2 2D materials

Two-dimensional (2D) materials are crystals having layered structure, single atomically thin layer could be exfoliated from the bulk 2D materials. For the exfoliated 2D layered material,

due to its atomically thin property, they could be employed for the creation of heterostructure.[24-27] The heterostructure could be made by either stacking layer by layer or by incorporating with nanostructure. 2D materials could be divided into three categories according to the band structures, 2D semimetal, 2D semiconductor and 2D insulator. In 2004, the zero bandgap 2D semimetal graphene was discovered by being isolated from the graphite with Scotch tape.[22] After the discovery of graphene, more and more 2D materials are gradually emerge including 2D semiconductor transition metal dichalcogenide (TMD) material and the 2D insulator hexagonal boron nitride (hBN). [23]

The 2D semiconductor materials like $MoS_2$, $WS_2$ and $WSe_2$ have attracted great interest due to their unique electronic and optical properties. Many of the 2D semiconductors are stable at ambient conditions.[28-29] 2D semiconductors could be easily synthesized either by bottom-up methods (e.g. chemical vapor deposition, molecular beam epitaxy) or by top-down methods (e.g. mechanical exfoliation, chemical exfoliation, laser and plasma thinning).[30-38] 2D semiconductors have been employed to fabricate hot electron device and achieve excellent performance, and they also have been utilized to harvest hot electrons. [20, 39-41] The time-resolved experiment shows that the process of the hot electron transfer between the plasmonic nanostructure and the 2D semiconductors is fast, on the order of 200 fs, which is beneficial in hot electron harvesting.[42]

Since 2D semiconductors are good materials for hot electron harvesting, this dissertation employed 2D semiconductors to extract hot electrons from the plasmonic nanostructure. Monolayer TMDs have direct bandgap emission while few-layer TMDs have indirect bandgap emission, because the indirect conduction band edge shifts to lower energy level with increasing number of layers.[43-47] And since the photoluminescence is closely related to the band gap and the electron doping level, with the unique properties of 2D semiconductors such as strong photoluminescence, large excitonic binding energy and allowing for the creation of heterostructure, in this dissertation we designed the heterostructures formed between plasmonic nanostructures and 2D semiconductors as a model system to study, and the photoluminescence spectroscopic

studies are sued to probe the hot electron transfer process. [21, 48-52] This dissertation aims at providing insights into the hot electron transfer mechanism between the metal and the semiconductor, including the hot electron injection direction and the modulation of hot electron transfer.

### 1.3 References


1. Yang, A., Wang, D., Wang, W., & Odom, T. W. (2017). Coherent Light Sources at the Nanoscale. *Annual Review of Physical Chemistry*, *68*(1), 83-99.
2. Zhang, Y., He, S., Guo, W., Hu, Y., Huang, J., Mulcahy, J. R., & Wei, W. D. (2017). Surface-Plasmon-Driven Hot Electron Photochemistry. *Chemical Reviews*, *118*(6), 2927-2954
3. Shan, H., Yu, Y., Wang, X., Luo, Y., Zu, S., Du, B., & Fang, Z. (2019). Direct observation of ultrafast plasmonic hot electron transfer in the strong coupling regime. *Light: Science & Applications*, *8*(1).
4. Tisdale, W. A., Williams, K. J., Timp, B. A., Norris, D. J., Aydil, E. S., & Zhu, X. Y. (2010). Hot-Electron Transfer from Semiconductor Nanocrystals. *Science*, *328*(5985), 1543-1547.
5. Wu, K., Chen, J., McBride, J. R., & Lian, T. (2015). Efficient hot-electron transfer by a plasmon-induced interfacial charge-transfer transition. *Science*, *349*(6248), 632-635.
6. Yang, A., Wang, D., Wang, W., & Odom, T. W. (2017). Coherent Light Sources at the Nanoscale. *Annual Review of Physical Chemistry*, *68*(1), 83-99.
7. Atwater, H. A., & Polman, A. (2010). Plasmonics for improved photovoltaic devices. *Nature Materials*, *9*(3), 205-213.
8. Clavero, C. (2014). Plasmon-induced hot-electron generation at nanoparticle/metal-oxide interfaces for photovoltaic and photocatalytic devices. *Nature Photonics*, 8(2), 95-103.

9. Linic, S., Christopher, P., & Ingram, D. B. (2011). Plasmonic-metal nanostructures for efficient conversion of solar to chemical energy. *Nature Materials*, *10*(12), 911-921.
10. Mubeen, S., Lee, J., Singh, N., Krämer, S., Stucky, G. D., & Moskovits, M. (2013). An autonomous photosynthetic device in which all charge carriers derive from surface plasmons. *Nature Nanotechnology*, *8*(4), 247-251.
11. Liu, Z., Hou, W., Pavaskar, P., Aykol, M., & Cronin, S. B. (2011). Plasmon Resonant Enhancement of Photocatalytic Water Splitting Under Visible Illumination. *Nano Letters*, *11*(3), 1111-1116.
12. Christopher, P., Xin, H., & Linic, S. (2011). Visible-light-enhanced catalytic oxidation reactions on plasmonic silver nanostructures. *Nature Chemistry*, *3*(6), 467-472.
13. Marimuthu, A., Zhang, J., & Linic, S. (2013). Tuning Selectivity in Propylene Epoxidation by Plasmon Mediated Photo-Switching of Cu Oxidation State. *Science*, *339*(6127), 1590-1593.
14. Knight, M. W., Sobhani, H., Nordlander, P., & Halas, N. J. (2011). Photodetection with Active Optical Antennas. *Science*, *332*(6030), 702-704.
15. Brongersma, M. L., Halas, N. J., & Nordlander, P. (2015). Plasmon-induced hot carrier science and technology. *Nature Nanotechnology*, *10*(1), 25-34.
16. Tian, Y., & Tatsuma, T. (2005). Mechanisms and Applications of Plasmon-Induced Charge Separation at TiO2 Films Loaded with Gold Nanoparticles. *Journal of the American Chemical Society*, *127*(20), 7632-7637.
17. White, T. P., & Catchpole, K. R. (2012). Plasmon-enhanced internal photoemission for photovoltaics: Theoretical efficiency limits. *Applied Physics Letters*, *101*(7), 073905.
18. Christopher, P., Xin, H., & Linic, S. (2011). Visible-light-enhanced catalytic oxidation reactions on plasmonic silver nanostructures. Nature Chemistry, 3(6), 467-472.

19. Mubeen, S., Lee, J., Singh, N., Krämer, S., Stucky, G. D., & Moskovits, M. (2013). An autonomous photosynthetic device in which all charge carriers derive from surface plasmons. *Nature Nanotechnology*, *8*(4), 247-251.
20. Wang, W., Klots, A., Prasai, D., Yang, Y., Bolotin, K. I., & Valentine, J. (2015). Hot Electron-Based Near-Infrared Photodetection Using Bilayer MoS2. *Nano Letters*, *15*(11), 7440-7444.
21. He, K., Kumar, N., Zhao, L., Wang, Z., Mak, K. F., Zhao, H., & Shan, J. (2014). Tightly Bound Excitons in MonolayerWSe2. *Physical Review Letters*, *113*(2).
22. Novoselov, K. S. (2004). Electric Field Effect in Atomically Thin Carbon Films. *Science*, *306*(5696), 666-669.
23. Mak, K. F., Lee, C., Hone, J., Shan, J., & Heinz, T. F. (2010). Atomically ThinMoS2: A New Direct-Gap Semiconductor. *Physical Review Letters*, *105*(13).
24. Geim, A. K., & Grigorieva, I. V. (2013). Van der Waals heterostructures. *Nature*, *499*(7459), 419-425.
25. Jariwala, D., Marks, T. J., & Hersam, M. C. (2016). Mixed-dimensional van der Waals heterostructures. *Nature Materials*, *16*(2), 170-181.
26. Wang, X., & Xia, F. (2015). Stacked 2D materials shed light. *Nature Materials*, *14*(3), 264-265.
27. Iannaccone, G., Bonaccorso, F., Colombo, L., & Fiori, G. (2018). Quantum engineering of transistors based on 2D materials heterostructures. *Nature Nanotechnology*, *13*(3), 183-191.
28. Novoselov, K. S., Mishchenko, A., Carvalho, A., & Castro Neto, A. H. (2016). 2D materials and van der Waals heterostructures. *Science*, *353*(6298), aac9439.
29. Li, X., Magnuson, C. W., Venugopal, A., An, J., Suk, J. W., Han, B., & Ruoff, R. S. (2010). Graphene Films with Large Domain Size by a Two-Step Chemical Vapor Deposition Process. *Nano Letters*, *10*(11), 4328-4334.

30. Graphene Films with Large Domain Size by a Two-Step Chemical Vapor Deposition Process. *Nano Letters*, *10*(11), 4328-4334.
31. Lee, Y., Zhang, X., Zhang, W., Chang, M., Lin, C., Chang, K., & Lin, T. (2012). Synthesis of Large-Area MoS2Atomic Layers with Chemical Vapor Deposition. *Advanced Materials*, *24*(17), 2320-2325.
32. Diaz, H. C., Chaghi, R., Ma, Y., & Batzill, M. (2015). Molecular beam epitaxy of the van der Waals heterostructure MoTe 2 on MoS 2 : phase, thermal, and chemical stability. *2D Materials*, *2*(4), 044010.
33. Li, H., Wu, J., Yin, Z., & Zhang, H. (2014). Preparation and Applications of Mechanically Exfoliated Single-Layer and Multilayer MoS2 and WSe2 Nanosheets. *Accounts of Chemical Research*, *47*(4), 1067-1075.
34. Backes, C., Berner, N. C., Chen, X., Lafargue, P., LaPlace, P., Freeley, M., & McDonald, A. R. (2015). Functionalization of Liquid-Exfoliated Two-Dimensional 2H-MoS2. *Angewandte Chemie*, *127*(9), 2676-2680.
35. Jawaid, A., Nepal, D., Park, K., Jespersen, M., Qualley, A., Mirau, P., & Vaia, R. A. (2015). Mechanism for Liquid Phase Exfoliation of MoS2. *Chemistry of Materials*, *28*(1), 337-348.
36. Lu, W., Nan, H., Hong, J., Chen, Y., Zhu, C., Liang, Z., Ma, X., Ni, Z., Jin C. & Zhang, Z. (2014). Plasma-assisted fabrication of monolayer phosphorene and its Raman characterization. *Nano Research*, *7*(6), 853-859.
37. Liu, Y., Nan, H., Wu, X., Pan, W., Wang, W., Bai, J., Zhao, W., Sun, L., Wang, X., Ni, Z. (2013). Layer-by-Layer Thinning of MoS2 by Plasma. *ACS Nano*, *7*(5), 4202-4209.
38. Chen, Y., Li, Y., Zhao, Y., Zhou, H., & Zhu, H. (2019). Highly efficient hot electron harvesting from graphene before electron-hole thermalization. *Science Advances*, *5*(11), eaax9958.

39. Liu, W., Li, L., Guo, H., Qadir, A., Bodepudi, S. C., Shehzad, K., Chen, W., Xie, Y., Wang, X., Yu, B., Xu, Y. (2019). Approaching the Collection Limit in Hot Electron Transistors with Ambipolar Hot Carrier Transport. *ACS Nano*, *13*(12), 14191-14197.

40. Torres, C. M., Lan, Y., Zeng, C., Chen, J., Kou, X., Navabi, A., Tang, J., Montazari, M., Adleman, J., Lerner, M., Zhong, Y., Li, L., Chen, C., Wang, K. L. (2015). High-Current Gain Two-Dimensional MoS2-Base Hot-Electron Transistors. *Nano Letters*, *15*(12), 7905-7912.

41. Yu, Y., Ji, Z., Zu, S., Du, B., Kang, Y., Li, Z., Zhou, Z., Shi, K., Fang, Z. (2016). Ultrafast Plasmonic Hot Electron Transfer in Au Nanoantenna/MoS2Heterostructures. *Advanced Functional Materials*, *26*(35), 6394-6401.

42. Tongay, S., Zhou, J., Ataca, C., Lo, K., Matthews, T. S., Li, J., Grossman, J., Wu, J. (2012). Thermally Driven Crossover from Indirect toward Direct Bandgap in 2D Semiconductors: MoSe2 versus MoS2. *Nano Letters*, *12*(11), 5576-5580.

43. Zhao, W., Ribeiro, R. M., Toh, M., Carvalho, A., Kloc, C., Castro Neto, A. H., & Eda, G. (2013). Origin of Indirect Optical Transitions in Few-Layer MoS2, WS2, and WSe2. *Nano Letters*, *13*(11), 5627-5634.

44. Amani, M., Lien, D., Kiriya, D., Xiao, J., Azcatl, A., Noh, J., Madhvapathy, S., Addou, R., KC, S., Dubey, M., Cho, K., Wallace, R., Lee, S., He, J., Ager, J., Zhang, X., Yablonovitch, E., Javey, A. (2015). Near-unity photoluminescence quantum yield in MoS2. *Science*, *350*(6264), 1065-1068.

45. Kim, H., Ahn, G. H., Cho, J., Amani, M., Mastandrea, J. P., Groschner, C. K., Lien, D. H., Zhao, Y., Ager, J. W., Scott, M. C., Chrzan, D. C., Javey, A. (2019). Synthetic WSe2 monolayers with high photoluminescence quantum yield. *Science Advances*, *5*(1), eaau4728.

46. Chernikov, A., Berkelbach, T. C., Hill, H. M., Rigosi, A., Li, Y., Aslan, O. B., Reichman, D. R., Hybertsen, M. S., Heinz, T. F. (2014). Exciton Binding Energy and Nonhydrogenic Rydberg Series in Monolayer WS2. *Physical Review Letters*, *113*(7).
47. Jiang, Z., Liu, Z., Li, Y., & Duan, W. (2017). Scaling Universality between Band Gap and Exciton Binding Energy of Two-Dimensional Semiconductors. *Physical Review Letters*, *118*(26).
48. Hanbicki, A., Currie, M., Kioseoglou, G., Friedman, A., & Jonker, B. (2015). Measurement of high exciton binding energy in the monolayer transition-metal dichalcogenides WS2 and WSe2. *Solid State Communications*, *203*, 16-20.
49. Huo, N., Kang, J., Wei, Z., Li, S., Li, J., & Wei, S. (2014). Novel and Enhanced Optoelectronic Performances of Multilayer MoS2-WS2 Heterostructure Transistors. *Advanced Functional Materials*, *24*(44), 7025-7031.
50. Li, Y., Cain, J. D., Hanson, E. D., Murthy, A. A., Hao, S., Shi, F., Li, Q., Wolverton, C., Chen, X., Dravid, V. P. (2016). Au@MoS2 Core–Shell Heterostructures with Strong Light–Matter Interactions. *Nano Letters*, *16*(12), 7696-7702.

## Chapter 2 : Hot Electron Transfer in Model System of Gold and $WSe_2$

### 2.1 Introduction

As mentioned in Chapter 1 Section 1.1, the metal and semiconductor interfaces are very important in the hot electrons application. Martin Moskovits *et al.* used the gold and $TiO_2$ system and realized the autonomous photosynthesis device, Jeong Young Park et al. incorporated gold and $Cu_2O$ and Xinghua Xia *et al.* used the gold and $MoS_2$ system to catalyze the water splitting reaction.[1-3] Electron transfer dynamics studies have been done on the metal and semiconductor interface including the using the transient spectroscopy to measure the electron transfer time scale.[4-12] However, the relationship between the hot electron transfer and the band structure has not yet been studied. From Chapter 1 Section 1.2 shows that 2D semiconductor layered materials have rich band transition possibilities due to their unique band structure properties as well as high quantum yield (when properly treated, the quantum yield for CVD synthesized $WSe_2$ could reach 60%).[13-15] Moreover, their band structure is easily tuned by using different growing parameters. In this chapter, the 2D semiconductor $WSe_2$ is used as a “probe” to study the hot electron transfer mechanism.

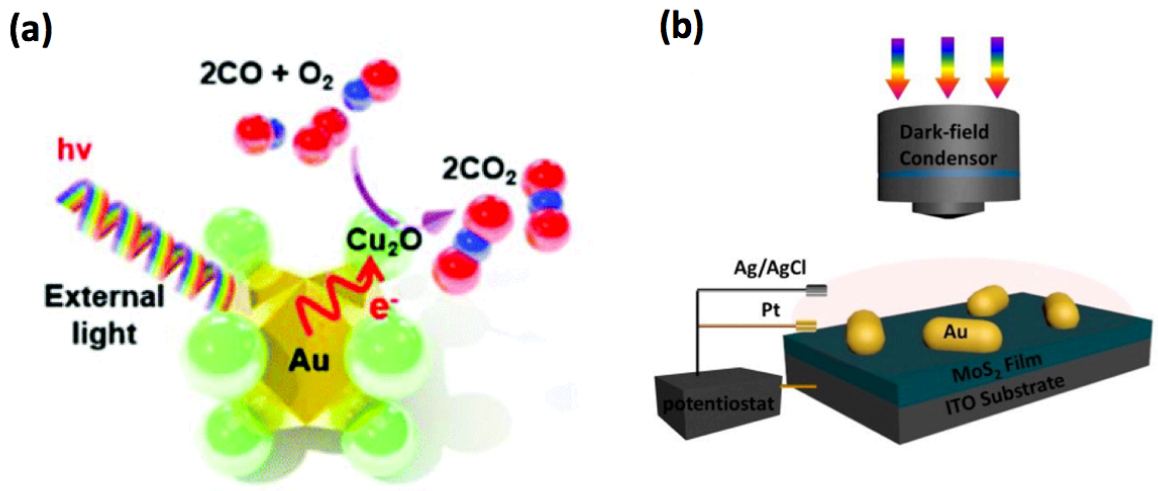


**Figure 2.1** (a) gold and $Cu_2O$ composite for CO oxidation.[2] Adapted from Ref. 2 with permission from the Royal Society of Chemistry. (b) Gold and $MoS_2$ for water splitting catalyst.[4] Adapted with permission from Ref. 4. Copyright © 2017, American Chemical Society.

The photoluminescence of $WSe_2$ have been widely studied, including the two-particle exciton, three-particle trion and four-particle biexciton, due to the strong Coulomb mediated many-body interaction.[15-23] Trion and biexciton are normally observed at low temperature, Jie Shan *et al.* observed the trion from monolayer $MoS_2$ at 10 K, Tony Heinz *et al.* observed biexciton from monolayer $WSe_2$ at 10 K.[16-17] Exciton is the bound state of electron and hole attracted to each other by Coulomb force. Since the biexciton and the trion states are not directly related to the band structure, and since in the metal-semiconductor junction, the plasmonic hot electrons inject into the conduction band of the semiconductor, which means that the hot electron injection should be closely related to the band structure. In this dissertation, we performed the experiments at room temperature, so if there are extra peak observed, we could safely exclude the trion or biexciton as the reasons. For the following sections, we used the model system of gold thin film

and $WSe_2$, and performed the spectroscopy measurements at room temperature to study the hot electron injection mechanism.

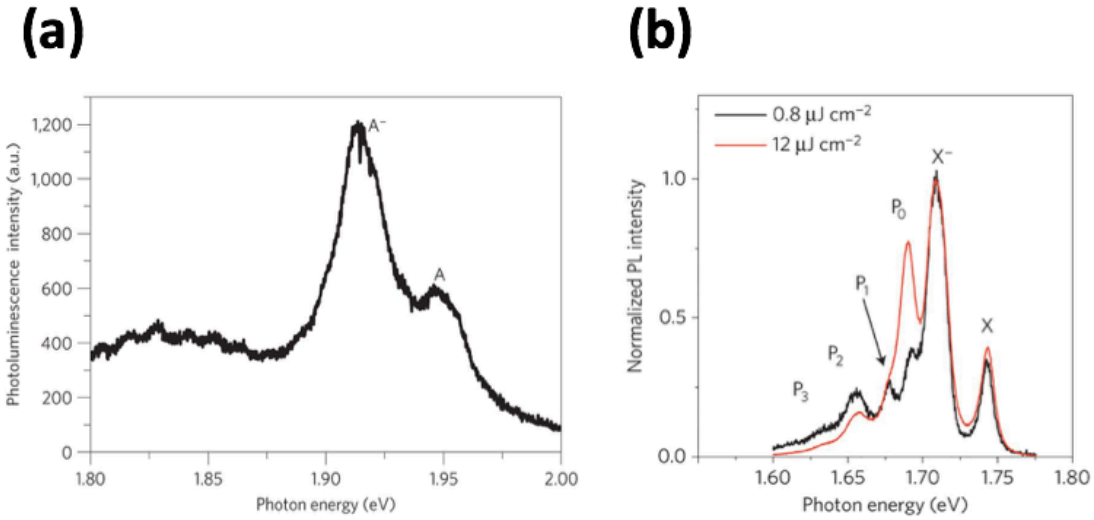


**Figure 2.2** (a) Photoluminescence spectrum of $MoS_2$ at 10 K, A- is trion peak, A is exciton peak.[16] Adapted with permission from Ref. 16. Copyright © 2013, Springer Nature. (b) Photoluminescence spectrum of $WSe_2$ with different laser fluence, X is exciton peak, $X^-$ is trion peak, $P_0$ is biexciton peak, $P_1$-$P_3$ are defect peaks. [17] Adapted with permission from Ref. 17. Copyright © 2015, Springer Nature.

For the few-layer $WSe_2$, there are three possible electron hole pair pathways at room temperature. Figure 2.3 (a) shows the band structure of few-layer $WSe_2$, of the three possible pathways, two are indirect transitions $K \rightarrow \Gamma$ and $\Lambda \rightarrow \Gamma$, and one is direct transition $K \rightarrow K$.[23] Figure 2.3 (b) is the photoluminescence spectra with different temperatures, which shows that amongst the three possible transitions, at room temperature, only two possible transitions: A ($K \rightarrow K$) direct transition

and $I_1$ ($K \rightarrow \Gamma$) indirect transition would observed. In the following section, we used these three possible transitions to study the hot electron injection mechanism.

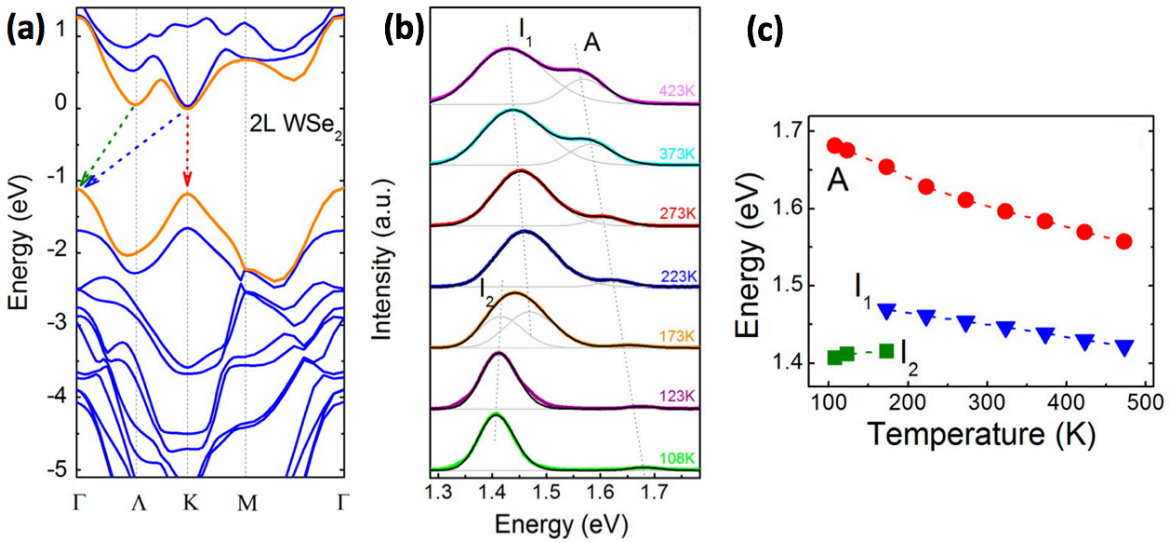


**Figure 2.3** (a) Few-layer $WSe_2$ band structure. The dashed arrows indicate the possible transition pathways ($K \rightarrow K$, $K \rightarrow \Gamma$, and $\Lambda \rightarrow \Gamma$) for excitons. The bands forming the conduction band minimum and valence band maximum are indicated in orange.[23] (b) Photoluminescence spectra at different temperatures. [23] (c) Photoluminescence peak positions as a function of temperature. [23] Adapted with permission from Ref. 23. Copyright © 2013, American Chemical Society.

## 2.2 Experimental

### 2.2.1 Material Fabrication and Characterization

The semiconductor 2D material $WSe_2$ fakes were synthesized with the CVD (chemical vapor deposition) method. [24] The reaction took place in a quartz tube with 1-inch diameter in the 12-inch horizontal tube furnace (Lindberg Blue M) (Figure 2.3). 0.6 g $WSe_2$ powder was put onto the alumina combustion boat. A 2 x 2 cm 300 nm $SiO_2$/Si wafer with silicon oxide was placed at 5 cm away from the combustion boat at the gas down-stream side. The $WSe_2$ powder boat was placed at the center of the hitting zone of the furnace. The furnace was heated up to 750 $^{o}$C, and

the growth would take place as it reached the melting point of the $WSe_2$ powder. The argon gas was continuously supplied into the furnace at the flow of 100 sccm (standard cubic centimeters per minute). After the growth last for 30 min, the heating process stop, and after which it was cooled down to room temperature before we stopped the argon gas supply and took the sample out from the furnace. With the CVD growing method, we were able to get the monolayer $WSe_2$ as well as the few-layer $WSe_2$ by tuning the growing parameters such as argon supply, and growing time.

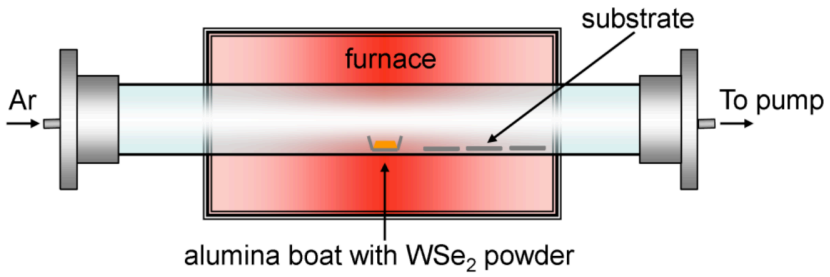


**Figure 2.4** Schematic illustration of the CVD furnace setup design for the growth $WSe_2$ furnace. A 1-inch diameter quartz tube displays the relative locations of substrate and powder.[24] Adapted from Ref. 24.

To confirm the structure and the properties of the as-grown few-layer $WSe_2$, we took the optical image, the Raman spectrum as well as the photoluminescence spectrum of the sample. Figure 2.4 (a) the optical image of the as grown few-layer $WSe_2$ flake showed that diameter is about 50 – 60 μm. From the contrast in the optical image the flake was a few-layer $WSe_2$ flake. The shape of the flake was triangle, which corresponded to the hexagonal crystal structure of $WSe_2$.[25-26] On the $SiO_2$/Si substrate, most of the flakes had triangular shape only a few had hexagonal shape. The reason is that for the CVD growth sample, the ratio of the tungsten and selenium might not be exactly 1:2 leading to the edges of the flakes were either tungsten terminated or selenium terminated.[27] Figure 2.4 (b) took $MoS_2$ as an example to show how the

atomic ratio had an impact on the shape of the flake, since $WSe_2$ had the same crystal structure as $MoS_2$, and they are composed of elements from the same periodic groups, the structure property of $MoS_2$ could be extendable to $WSe_2$.[28-32] Figure 2.5 (a) showed the Raman spectrum of the as-grown sample, the Raman peak was at 250 $cm^{-1}$, which corresponded to the Raman out-of-plane $A_{1g}$ and in-plane $E_{2g}$ vibrational modes in the literature, $WSe_2$ has the two vibrational modes at the same wavenumber.[33-37] Figure 2.6 showed the photoluminescence spectrum of the as-grown $WSe_2$ flake, there was one peak at 760 nm, which according to the literature corresponds to the $I_1$ indirect transition from the $\Lambda$ point to $\Gamma$ point, which further confirmed that the sample was the few-layer sample, because due to the band structure difference, the monolayer sample would show the direct transition A transition instead of the indirect transition.[23]

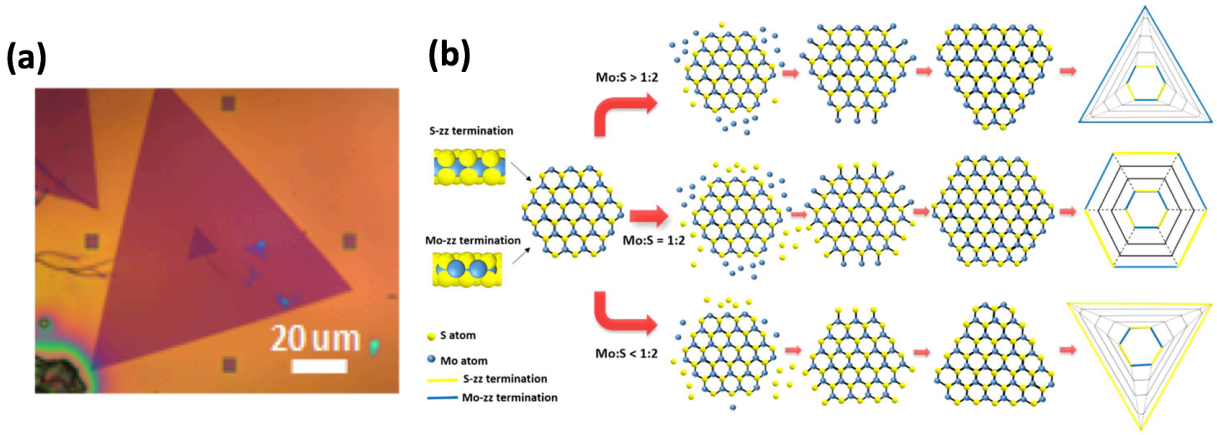


**Figure 2.5** (a) Optical image of the as-grown few-layer $WSe_2$. (b) Schematic illustration of the relationship between Mo:S atomic ratio and the flake shape.[28] Adapted with permission from Ref. 28. Copyright © 2014, American Chemical Society.

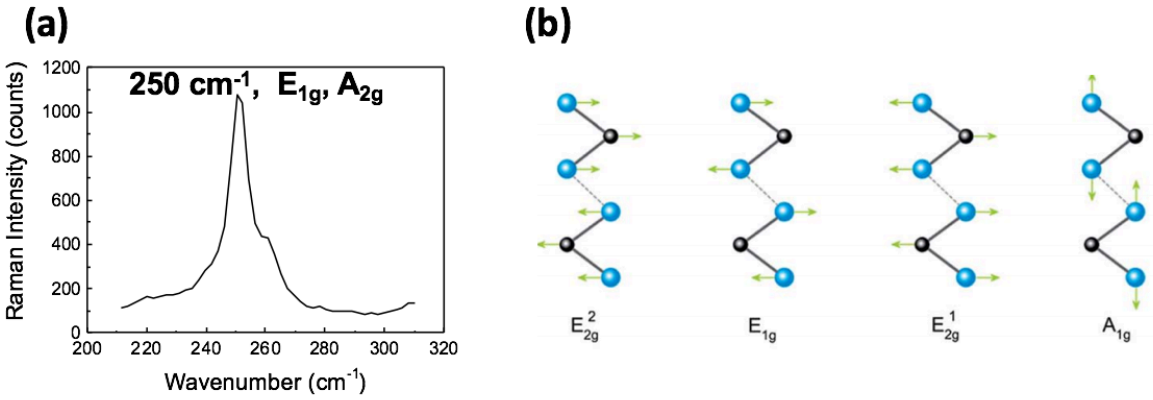


**Figure 2.6** (a) Raman spectrum of few-layer $WSe_2$. (b) Raman active and two inactive vibrational modes of the transition metal dichalcogenides $MX_2$ (M = Mo, W and X = Se, S).[33] Adapted from Ref. 33. Adapted with permission from the Royal Society of Chemistry.

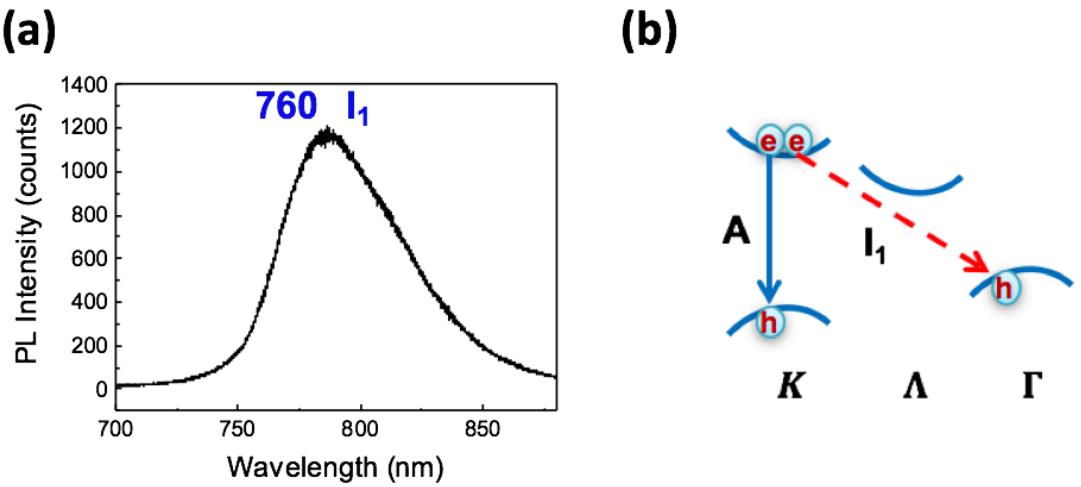


**Figure 2.7** (a) PL (photoluminescence) spectrum of few-layer $WSe_2$. (b) Schematic illustration of few-layer $WSe_2$ exciton relaxation pathways, A transition is direct band transition, $I_1$ transition is indirect band transition.

### 2.2.2 Material Wet Transfer for Gold-$WSe_2$ Model System

Our study model system was made of $WSe_2$ sitting on top of the gold thin film. The samples were made by transferring the few-layer $WSe_2$ onto the gold thin film with the assistant of the PMMA (polymethyl methacrylate) (PMMA A8 from MicroChem). The 40-nm gold thin film was evaporated onto the $SiO_2$/Si substrate by E-beam evaporation with the speed of 1 Å/s. For the $WSe_2$, after the CVD process the $WSe_2$ flakes spread on the $SiO_2$/Si substrate, and they needed to be transferred on top of the gold thin film. To lift the $WSe_2$ flakes from the substrate, wet etching was used to etch the oxide layer of the substrate so as to detach the PMMA with $WSe_2$ adhered underneath from the substrate. The wet transfer process is as follows (Figure 2.7): (1) The PMMA was spin-coated onto the $SiO_2$/Si substrate that have the as-grown $WSe_2$ with 4000 rmp, and then baked on the hot plate at 180 $^oC$ for 10 min, forming the PMMA layer with the thickness of about 600 nm; (2) The wet etchant was the 10% potassium hydroxide, gently placed the substrate with $WSe_2$ flakes and PMMA onto the etchant, then it was put into the oven to etch for 5 min at 120 $^oC$; (3) When the etching process finished, the PMMA with the $WSe_2$ flakes would float onto the etchant, leaving the substrate sunk in the etchant; (4) Tweezed a clean dry $SiO_2$/Si substrate and slowly approached the floating PMMA so as to let the PMMA flatten onto the substrate, immersed it in a beaker of the deionized water, the PMMA would float onto of the water, repeated this step for three times to rinse the residual etchant. (5) To transfer to the gold thin film, like the last step tweezed the $SiO_2$/Si substrate with gold thin film and slowly approached the floating PMMA, the PMMA with the $WSe_2$ would flatten onto the gold thin film, and let it dry in the fume hood for overnight. When it is dry, the PMMA with the $WSe_2$ would stick to the gold thin film without slipping.

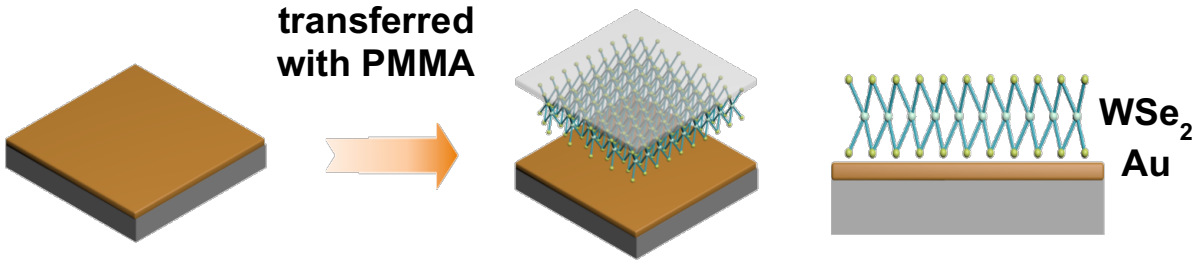


**Figure 2.8** Schematic illustration of PMMA assisted $WSe_2$ transfer process, during the transfer process $WSe_2$ flakes would adhere to the PMMA, and the PMMA with $WSe_2$ flakes would be flattened onto the gold thin film.

### 2.2.3 Spectrum Measurement

We excited the photoluminescence using the setup of confocal microscope with laser. The laser with the wavelength of 488 nm, and the power of 3 μW was used. The laser spot went through the band pass filter and ND-filter, and then the laser spot was focused onto the device. The band pass filter was used to filter the clean up the laser make it more monochromic. The ND-filter (neutral-density filter) was used to adjust the intensity of the laser, it controlled the intensity with 0.1%, 1%, 2.5%, 10%, 25%, 50% 100% transmissions. In the experiments, we used the ND-filter to adjust the laser intensity to study the laser intensity dependent spectrum response. With the beam splitter in the system, the spectrum is collected through the confocal lens, and then to the CCD (charge-coupled device) detector.

Figure 2.8 showed the photoluminescence generation and measurement process. The luminescence is generated by electron hole pair recombination. The electrons relax from the conduction band to the valence band of the semiconductor. In photoluminescence, the electron hole pair is generated by the excitation of laser. In the experiment, we focus laser onto the sample through the object lens, and the luminescence signal was collected in the same object lens but

collected signal would be reflected to the CCD collector of the spectrometer to collect photon counts. The photoluminescence spectra in this chapter and in the following chapters were taken using the method.

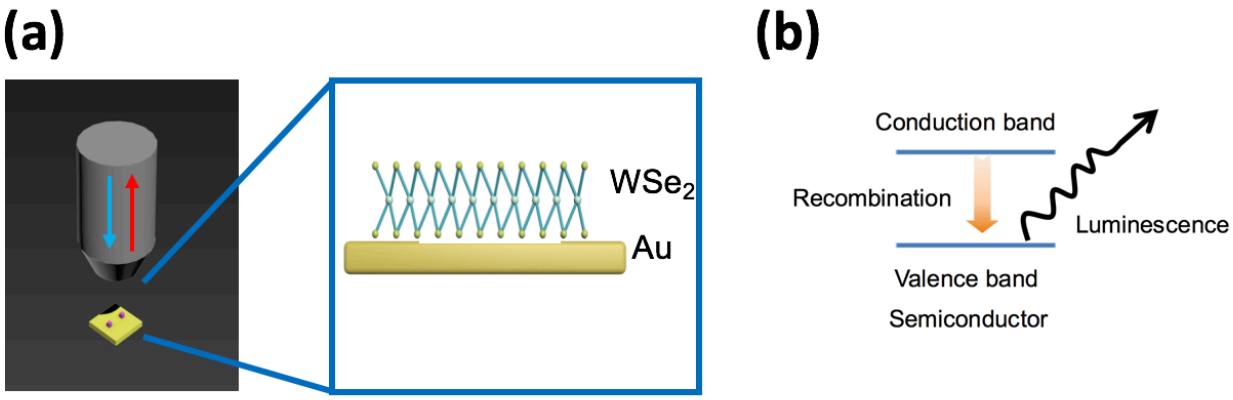


**Figure 2.9** Photoluminescence measurement setup and generation process. (a) Sample placed under the object lens, the blue arrow indicates the 488-nm laser injection, the red arrow indicates the collected luminescence. (b) Photoluminescence generation, electrons in the conduction band recombine with the holes in the valence band generating luminescence.

## 2.3 Results and Discussion

### 2.3.1 Observation and Assumption

We inspected the photoluminescence spectrum data of the sample, and we find out that for few-layer $WSe_2$ sample with the gold thin film as the hot electron sink, the collected data of sample has an extra photoluminescence peak, which we assumed that it was produced by the transferred hot electrons from the gold thin film hot electron sink to the few-layer $WSe_2$ (Figure 2.9). Moreover, since this phenomenon emergences at the few-layer $WSe_2$ samples instead of the monolayer $WSe_2$ samples, we assumed that this extra peak was also related to the indirect band transition. To prove our assumption, we do several control experiments to prove the

assumption and study the mechanism of the hot electron transfer between the hot electron sink and the few-layer $WSe_2$.

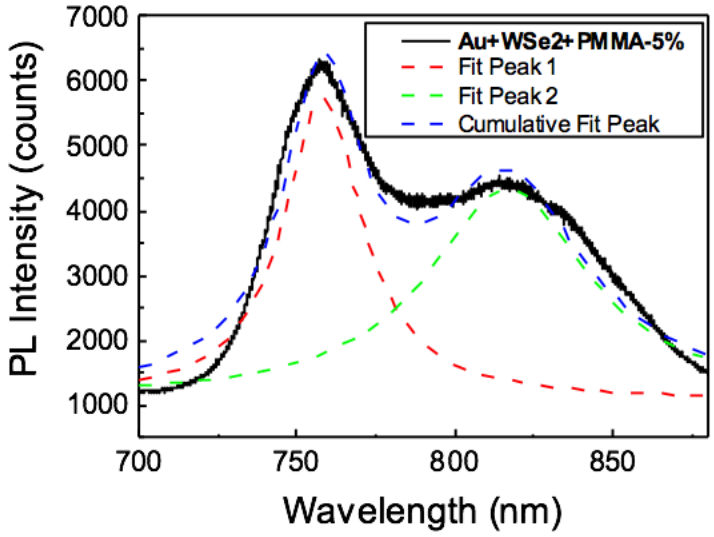


**Figure 2.10** Photoluminescence spectrum of as-grown $WSe_2$ transferred onto the gold thin film, the peak fit shows two peaks, one at between 745 – 760 nm, the other at 830 nm.

### 2.3.2 Control Experiments

Except for hot electron, like we mentioned in the introduction of this chapter, there are several reasons for the emergence of a new photoluminescence peak, which includes defect induced by the transfer process or negative trion consisting of two electrons and one hole. Firstly, the trion exciton peak assignment be excluded since we perform our experiment at room temperature. The trion exciton peak has small binding energy about 20 meV, which is smaller than 25 meV ($k_BT$ = 25 meV at room temperature T = 298 K), the trion exciton peak of the $WSe_2$ will not appear at room temperature.[38] In the following experiment, we are going to exclude the reason of defect luminescence.

To further confirm the emergence of the new peak was induced by the hot electron, we conducted several control experiments. The samples were made by transferring the few-layer $WSe_2$ onto the gold thin film with the assistant of the PMMA, and this process was performed by

etching the silicon oxide layer with the 10% potassium hydroxide for 5 min at 120 $^{o}$C, then the PMMA with the few-layer $WSe_2$ flakes were transferred onto the substrate with the gold thin film. During this process, defects might be introduced to the few-layer $WSe_2$ flakes and induce the photoluminescence. We used the same transfer process to transfer the flakes onto the silicon wafer without the gold thin film. And the photoluminescence spectrum did not show extra peak (Figure 2.10).

In another control experiment, we made a gold thin film bar, a few-layer $WSe_2$ flake was transferred onto the bar with the same wet etching transfer process so that part of the flake was placed onto the gold thin film strip, while the other part of it was placed onto the silicon wafer. We took the photoluminescence spectrum of this few-layer flake, and only the part of the flake onto the gold thin film had extra photoluminescence peak (Figure 2.11). Please note that in this experiment, since we were performing the experiment on the same flake, to avoid the signal from the other part of the flake mixing into the spectrum, we used lower laser intensity which led to lower photoluminescence counts. The optical image of the sample Figure 2.11 (a) showed two small thinner gold bar, this was to test if the width of the gold bar would have an effect on the spectrum. We found out that for area in the thinner gold bar, the spectrum didn't show two photoluminescence peaks. In the following experiments, we used the thin gold film instead of gold bar to reduce the parameters that would affect the electron transfer process. These two control experiments confirmed that the extra photoluminescence peak was not introduced by the defect. We could confirm that the hot electron transfer was the reason for the emergence of the extra photoluminescence peak, from which we studied the hot electron transfer mechanism.

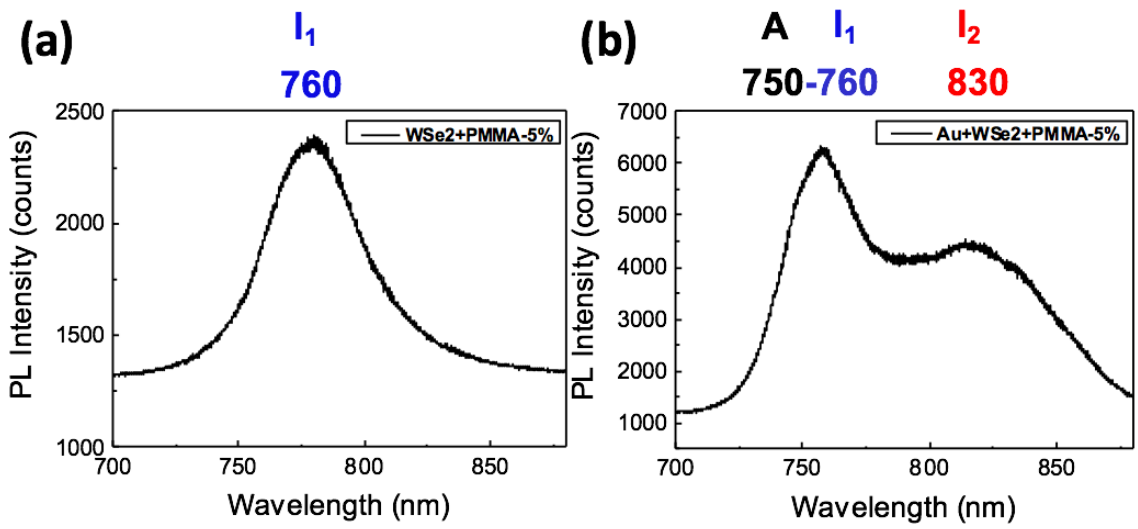


**Figure 2.11** (a) Photoluminescence spectrum of as-grown $WSe_2$ transferred onto the $SiO_2$/Si substrate. (b) Photoluminescence spectrum of as-grown $WSe_2$ transferred onto the gold thin film, the peak fit shows two peaks, one at between 745 – 760 nm, the other at 830 nm.

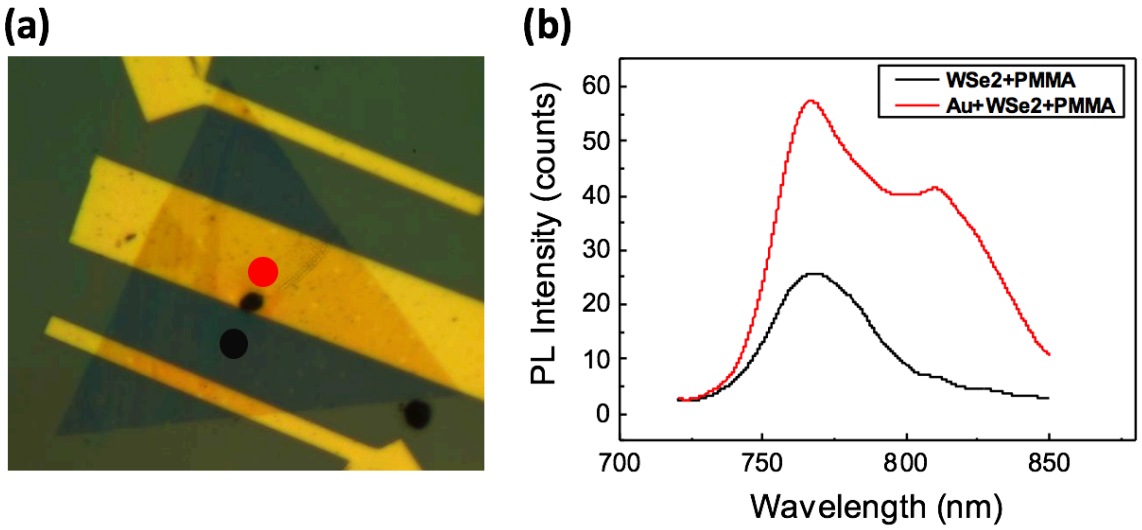


**Figure 2.12** (a) Optical image of a few-layer $WSe_2$ flake transferred onto a wide gold bar and two thin gold bars. (b) Photoluminescence spectra, the red curve is the spectrum for the red dot area in the optical image, the black curve is the spectrum for the black dot area in the optical image.

Since the spectra for the areas in the thin gold bars are the same as black dot area, their spectra are not showed here.

### 2.3.3 Hot Electron Transfer Mechanism

The control experiments from the last section, the hot electron transfer process is closely related to the indirect band transition of the 2D semiconductor materials. Before studying the mechanism of the hot electron transfer through the indirect band transition, we needed to look into the indirect transition of the 2D semiconductor. According the references, for few-layer $WSe_2$, there are three possible transitions related to $K$, $\Lambda$, $\Gamma$ points of the few-layer $WSe_2$.[23] For monolayer $WSe_2$, the direct transition is within the conduction band and the valence band of the $K$ valleys. For few-layer $WSe_2$, except for the direct transition within the $K$ valleys $K \rightarrow K$ (A transition, 745 nm), there are indirect transition pathways from $K \rightarrow \Gamma$ points ($I_1$ transition, 760 nm), and from $\Lambda \rightarrow \Gamma$ points ($I_2$ transition, 830 nm) respectively. At room temperature however, we could only observe the direct transition A ($K \rightarrow K$) transition and the indirect $I_1$ ($K \rightarrow \Gamma$) transition.

The photoluminescence spectrum of the few-layer $WSe_2$ on gold substrate showed that the two peaks were at 755 nm and 830 nm respectively. When compared to the peaks at the reference, we assign the peak at 830 nm as the $I_2$ ($\Lambda \rightarrow \Gamma$) transition. For the other peak (755 nm) that was at between 745 nm and 760 nm, according to the reference there possibly exists A ($K \rightarrow K$) transition and $I_1$ ($K \rightarrow \Gamma$) transition, we assigned this peak as the combination of A ($K \rightarrow K$) transition and $I_1$ ($K \rightarrow \Gamma$) transition (Figure 2.12). Here we put forward an assumption that the hot electrons inject into the $K$ and the $\Lambda$ valleys, which in turn increases the recombination rate of the $I_1$ ($K \rightarrow \Gamma$) transition and $I_2$ ($\Lambda \rightarrow \Gamma$) transition.

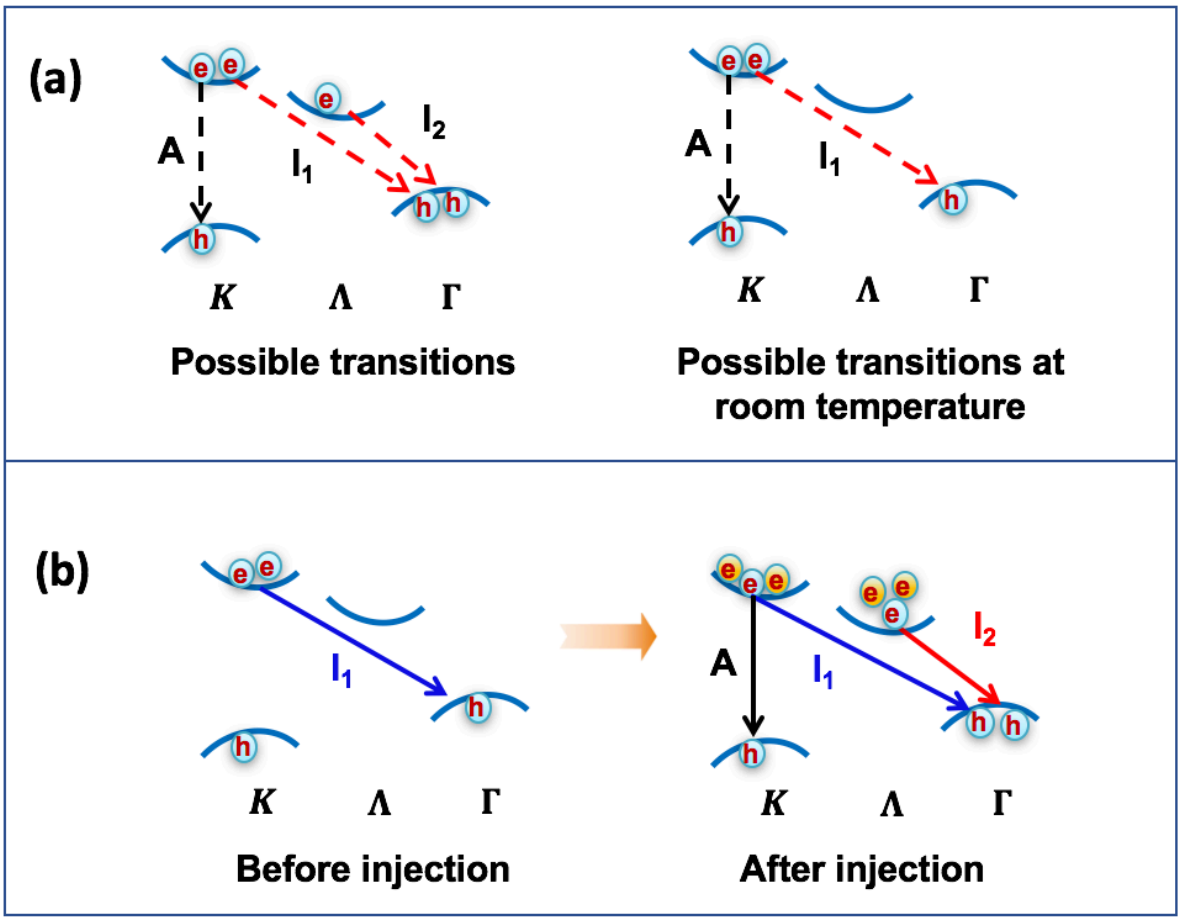


**Figure 2.13** Band structure illustrations: (a) All possible transitions and possible transitions at room temperature for few-layer $WSe_2$ at K, Λ and Γ points. Dash line indicates the possible transitions, black dash line indicates the direct transition, red dash line indicates the indirect transition. (b) Transitions as showed at the photoluminescence spectra, the yellow electron symbols represent the injected hot electrons. Before the hot electron injection, in the photoluminescence spectrum Figure 2.10 (a), $I_1$ (K→Γ) transition was observed. After the hot electron injection, in the photoluminescence spectrum Figure 2.10 (b), all the three transitions A (K→K), $I_1$ (K→Γ) and $I_2$ (Λ→Γ) transitions were observed.

We gave the assumption for the hot electron injection in Section 2.3.1 based on the observation, to prove our assumption as well as to figure out the mechanism of the hot electron

transfer process, we did the laser intensity dependent experiment. As we mentioned in the introduction part, the hot electron in the plasmonic materials are generated from the d-band of the gold with laser excitation, which means that with lower excitation intensity, the number of hot electrons will be lower, and with the increase in the laser intensity, the number of hot electrons will increase until it saturates. In this experiment, we adjusted the intensity of the laser by changing the ND filter in the spectrometer, and the intensity is changed from 0.1% to 5% of the generated laser intensity, and with different laser intensities, the number of hot electrons generated would be different. Figure 2.13 shows the stacked photoluminescence spectra with different laser intensity showed that, when the laser intensity is low, there are two photoluminescence peaks. One lies at the 745 nm which is the A ($K \rightarrow K$) transition, and the other one lies at 830 nm which is the $I_2$ ($\Lambda \rightarrow \Gamma$) transition. With the increase in the laser intensity, the peak at 745 nm gradually moves to between 745 nm to 760 nm. Please note that the figure below is the normalized intensity figure, for the actually photoluminescence spectra, the photoluminescence intensity increased. Since few-layer $WSe_2$ has only three possible transition at room temperature, that is A ($K \rightarrow K$), $I_1$ ($K \rightarrow \Gamma$), and $I_2$ ($\Lambda \rightarrow \Gamma$) transition. From the laser intensity dependent experiment, we could derive the hot electron injection mechanism, that is, (1) for the low amount of the hot electrons generated from the plasmonic materials, the hot electrons will inject into the $K$ valley and the $\Lambda$ valleys, and increase the recombination rate of the A ($K \rightarrow K$) and $I_2$ ($\Lambda \rightarrow \Gamma$) transition, (2) with more hot electrons inject into the semiconductor, the number of the hot electrons injected into the $K$ valley would increase, and thus the $I_1$ ($K \rightarrow \Gamma$) transition increases.

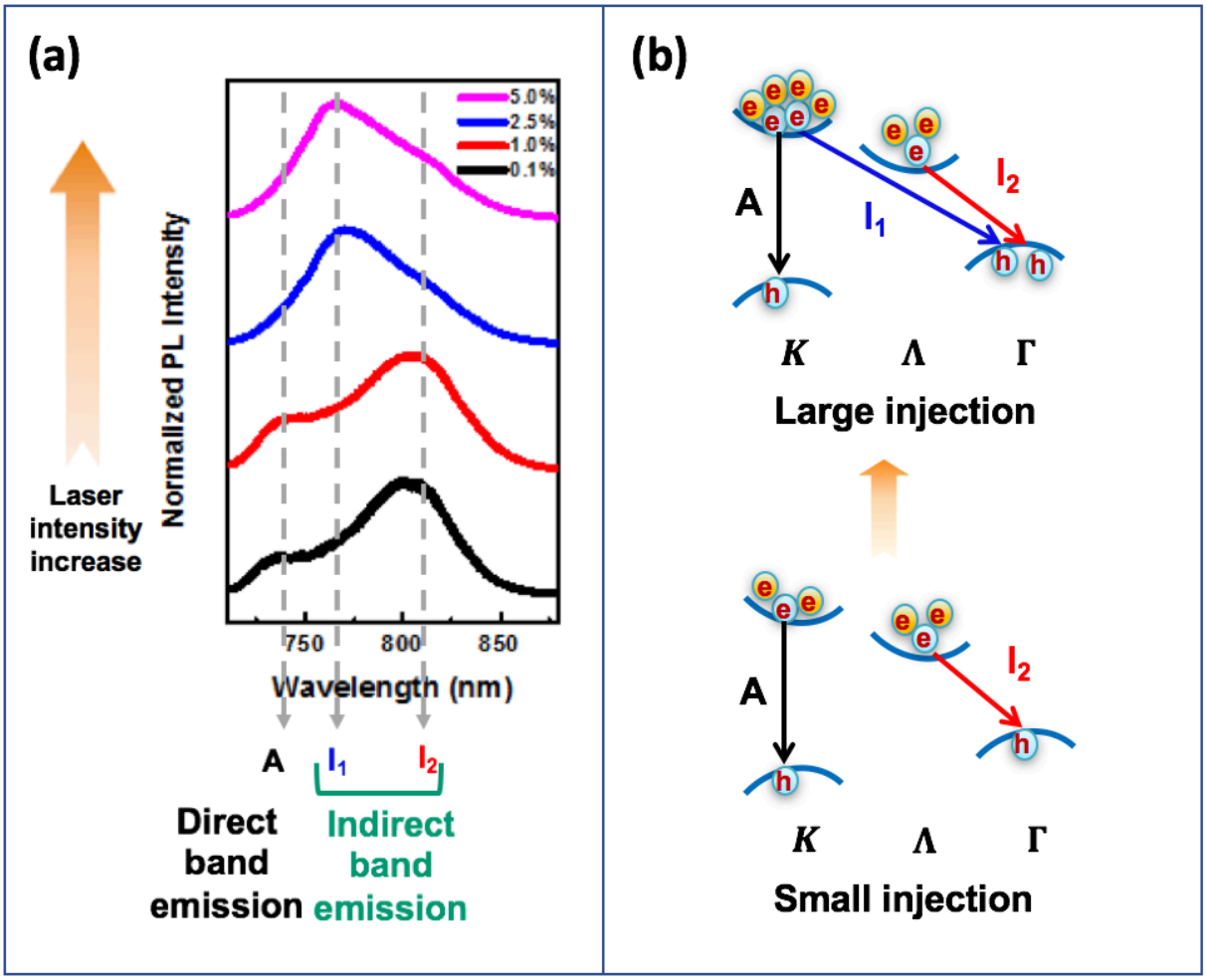


**Figure 2.14** (a) Normalized photoluminescence spectra of gold and few-layer $WSe_2$ model system under different laser intensities. (b) Schematic illustrations of the transition pathways between valleys of few-layer $WSe_2$, yellow electron symbols indicate injected hot electrons.

### 2.3.4 Photoluminescence Peak Splitting

To further support the proposed mechanism based on the laser intensity dependent experiment, we performed an experiment on the few-layer $WSe_2$ with different stacking angles. The model system for this experiment was the same, few-layer $WSe_2$ wet transferred on the gold thin film. What made this experiment different and interesting was that the few-layer $WSe_2$ were not the as-grown few-layer $WSe_2$ flakes, instead, to made the few-layer $WSe_2$, we transferred the

CVD-grown monolayer $WSe_2$ twice. According to the reference, stacking angles of the monolayer 2D semiconductors have great impact to the photoluminescence peaks due to the interaction between monolayers (Figure 2.14).[39-45] Different stacking angles lead to different distances between the two monolayers, which in turn would affect the layer interaction, and the photoluminescence peaks positions. The literature discussed the band structure of $MoS_2$ with different stacking angles, since $WSe_2$ and $MoS_2$ are made of elements from the same periodic groups, $WSe_2$ should also have the same properties with different stacking angles.

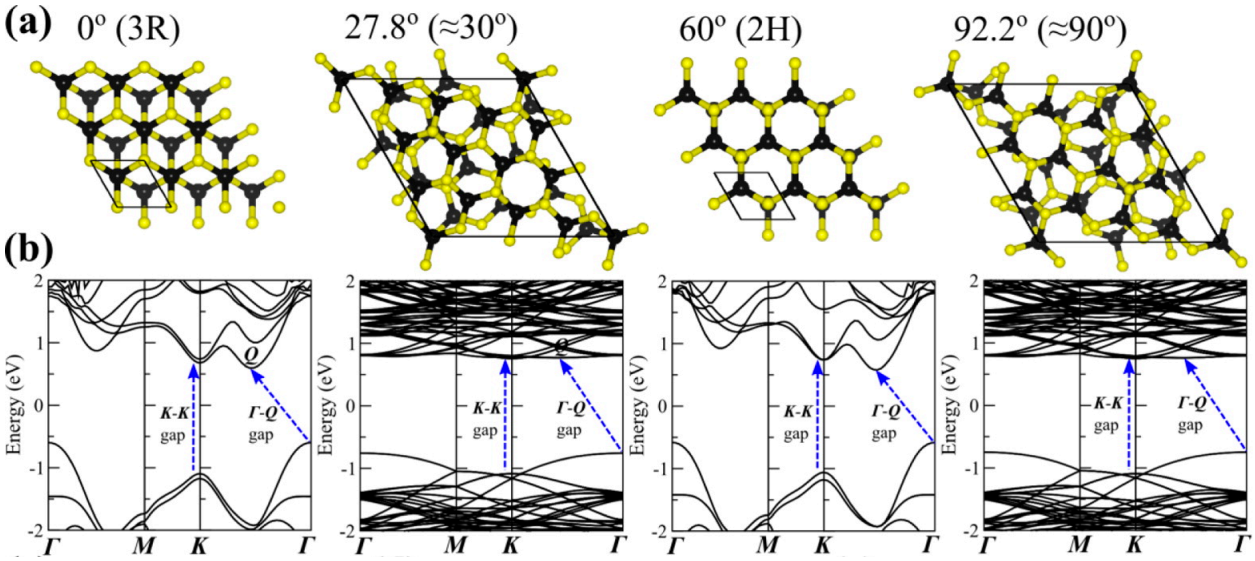


**Figure 2.15** (a) Illustrations atomic structure of $MoS_2$ with different stacking angles. The black solid line shows the unit cell. (b) DFT Band structures corresponding to atomic structures shown at (a).[39] Adapted with permission from Ref. 39. Copyright © 2014, American Chemical Society.

From the result of the laser intensity dependent experiment in the previous Section 2.3.2 and Section 2.3.3, we found out that the laser intensity of the A ($K \rightarrow K$) and $I_1$ ($K \rightarrow \Gamma$) transition photoluminescence peaks tend to merge into one peak, we could obtain more information and have more convincing supports if the peak could be split and clearly show two transitions, A ($K \rightarrow K$) and $I_1$ ($K \rightarrow \Gamma$). This experiment was based on the assumption that with by changing the stacking

angles the photoluminescence peaks positions would shift, so we expect to observe the peak between 745 nm and 760 nm splitting into two peaks, which would clearly indicate the A ($K \rightarrow K$) and $I_1$ ($K \rightarrow \Gamma$) transitions.

Since we were looking for the stacking angles that allowed us to observe the peak splitting, the exact stacking angle of the monolayers is not the research focus as long as we observed the splitting, in this experiment we used the optical image to roughly get the stacking angles. The as-grown monolayer $WSe_2$ is normally triangular or hexagonal due to the hexagon crystal structure, and the stacking angle could be obtained from the edges of the two monolayer samples. With the assumption we mentioned, the experiment was designed as follows: (1) Tune the parameters of the CVD growing process for $WSe_2$ to get the monolayer $WSe_2$; (2) With the assistant of PMMA transfer twice the monolayer $WSe_2$ onto the substrate with gold thin film, and between each transfer the sample was rotated so that the stacking angle was not zero; (3) Take the photoluminescence spectra of the samples; (4) Repeat the step (1)-(3) but change the substrate with $SiO_2$/Si substrate, this step was to create the control group for this experiment. Figure 2.15 shows the photoluminescence spectra of different stacking angles. At room temperature, there are two possible transitions, A ($K \rightarrow K$) and $I_1$ ($K \rightarrow \Gamma$) transitions (Figure 2.12). In Figure 2.15, for some spectra two peaks were observed, we could safely draw a conclusion that they correspond to the A ($K \rightarrow K$) and $I_1$ ($K \rightarrow \Gamma$) transitions.

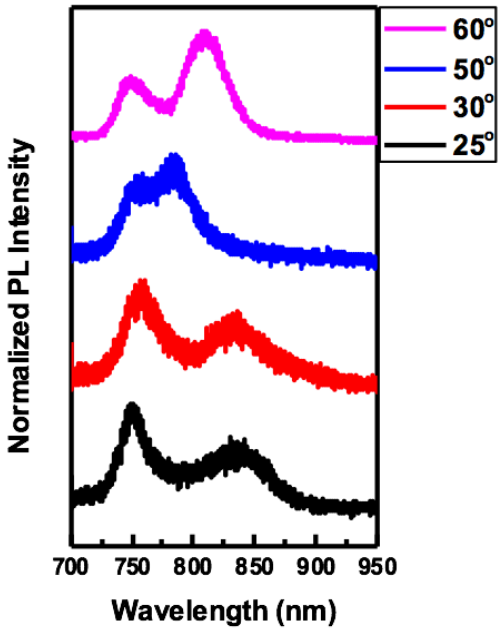


**Figure 2.16** Photoluminescence spectra of different stacking angles.

Figure 2.16 compared the photoluminescence spectra of the stacking few-layer $WSe_2$ flakes on the gold thin film and those of few-layer $WSe_2$ flakes on the $SiO_2$/Si substrate. In the photoluminescence spectrum of few-layer $WSe_2$ flakes the on gold thin film showed three luminescence peaks, while that of few-layer $WSe_2$ flakes on the $SiO_2$/Si substrate showed two luminescence peaks. According to the possible transitions of the 2D few-layer $WSe_2$ as well as the peak position (Figure 2.12), for the sample with gold thin film we could assign the three peaks from low wavelength to high wavelength as A ($K \rightarrow K$), $I_1$ ($K \rightarrow \Gamma$) and $I_2$ ($\Lambda \rightarrow \Gamma$) transition respectively. For the spectrum of the control sample on the $SiO_2$/Si substrate, there were two peaks, based on the positions of the peaks we assigned them as A ($K \rightarrow K$) and $I_1$ ($K \rightarrow \Gamma$) transitions. This experiment provided further supports for the hot electron transfer mechanism we put forward in the previous Section 2.3.3, that is the hot electrons inject into the $\Lambda$ valley, leading to the increased recombination rate of $I_2$ ($\Lambda \rightarrow \Gamma$) transition. The overlap area of the samples on

gold thin film showed three peaks (three transitions A ($K \rightarrow K$), $I_1$ ($K \rightarrow \Gamma$) and $I_2$ ($\Lambda \rightarrow \Gamma$) transitions), while the monolayer area showed only one peak (A ($K \rightarrow K$) direct transition).

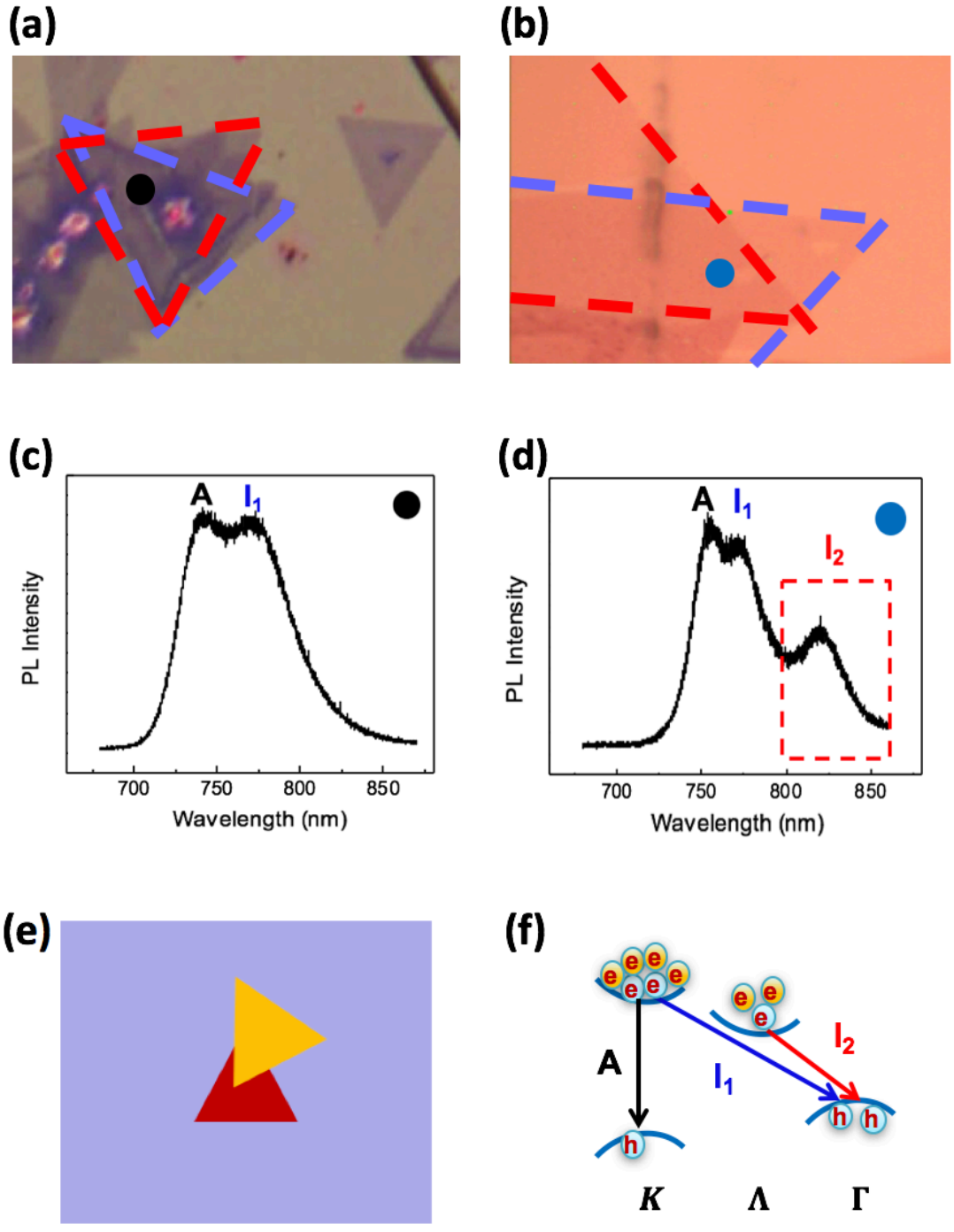


**Figure 2.17** (a) Optical image of transferred-few-layer $WSe_2$ on $SiO_2$/Si substrate. (b) Optical image of transferred-few-layer $WSe_2$ on gold thin film substrate. (c) Photoluminescence spectrum

of black dot area at (a). (d) Photoluminescence spectrum of blue dot area at (b). (e) Illustration of transferred-few-layer $WSe_2$, red area indicates the bottom monolayer $WSe_2$, yellow area indicates the top layer $WSe_2$. (f) Illustration of band structure of transferred-few-layer $WSe_2$, the arrows indicate the possible transitions, black arrow A ($K \rightarrow K$), blue arrow $I_1$ ($K \rightarrow \Gamma$), red arrow $I_2$ ($\Lambda \rightarrow \Gamma$).

### 2.3.5 Gold-$WSe_2$ Model System with Monolayer $WSe_2$

In the photoluminescence spectrum of the as-grown monolayer $WSe_2$, the direct transition is the only observed transition (A ($K \rightarrow K$) transition) at room temperature. To further prove that this photoluminescence phenomenon we observed in Section 2.3.1 was closely related to the indirect transition. We performed an experiment in the same model system but with monolayer $WSe_2$.

The experiment was designed as follows: (1) A thin gold bar is evaporated on the substrate; (2) An as-grown monolayer $WSe_2$ flake was transferred onto the gold bar substrate with the assistant of PMMA so that part of the flake was on the thin gold bar, and part of the flake not on the thin gold bar; (3) Did the photoluminescence mapping to the transferred monolayer $WSe_2$ flake.

The photoluminescence analysis of monolayer $WSe_2$ partly on the thin gold bar is showed in Figure 2.17. The photoluminescence spectrum Figure 2.17 (a) showed only one peak at about 745 nm, which is the position of A ($K \rightarrow K$) direct transition. Figure 2.17 (b) illustrated the band structure and transition pathway of monolayer $WSe_2$, when compared to the band structure of the few-layer $WSe_2$ (Figure 2.12), the difference is at the $\Lambda$ valley —— the monolayer $WSe_2$ has higher $\Lambda$ valley and it is higher than the $K$ valley of it, while the few-layer $WSe_2$ has lower $\Lambda$ valley and it is lower than the $K$ valley of it, and this is also the reason that monolayer only showed direct band transition.

The photoluminescence mapping (Figure 2.17 (c)(d)) showed that, for the part of the monolayer $WSe_2$ on the thin gold bar, the photoluminescence intensity was quenched, which was the opposite to the case of few-layer $WSe_2$. For monolayer $WSe_2$, the $\Lambda$ valley was higher than $K$ valley, so there was less probability for the hot electrons to inject into the $\Lambda$ valley. However, instead of increasing the photoluminescence intensity, the photoluminescence quenched for the monolayer $WSe_2$ on thin gold bar. Here we could make a conclusion that the hot electrons tend to inject into the $\Lambda$ valley of the few-layer $WSe_2$, because its $\Lambda$ valley has the valley level lower than that of the monolayer $WSe_2$, which leads to the increase to the recombination rate of the possible transitions of $WSe_2$. For the monolayer $WSe_2$ that have the $\Lambda$ valley higher than the $K$ valley, instead of recombining with the holes in the valence band, the electrons in the conduction band tend to back-transfer to the gold and thus quench the photoluminescence. This experiment gave us insights as to the relationship between the valley level and the hot electron injection rate. High valley level leads to low hot electron injection efficiency, and being in contact with gold makes the electrons transfer to the gold resulting in photoluminescence quenching, while low valley level leads to high hot electron injection efficiency, with more hot electrons accumulates, photoluminescence intensity would increase.

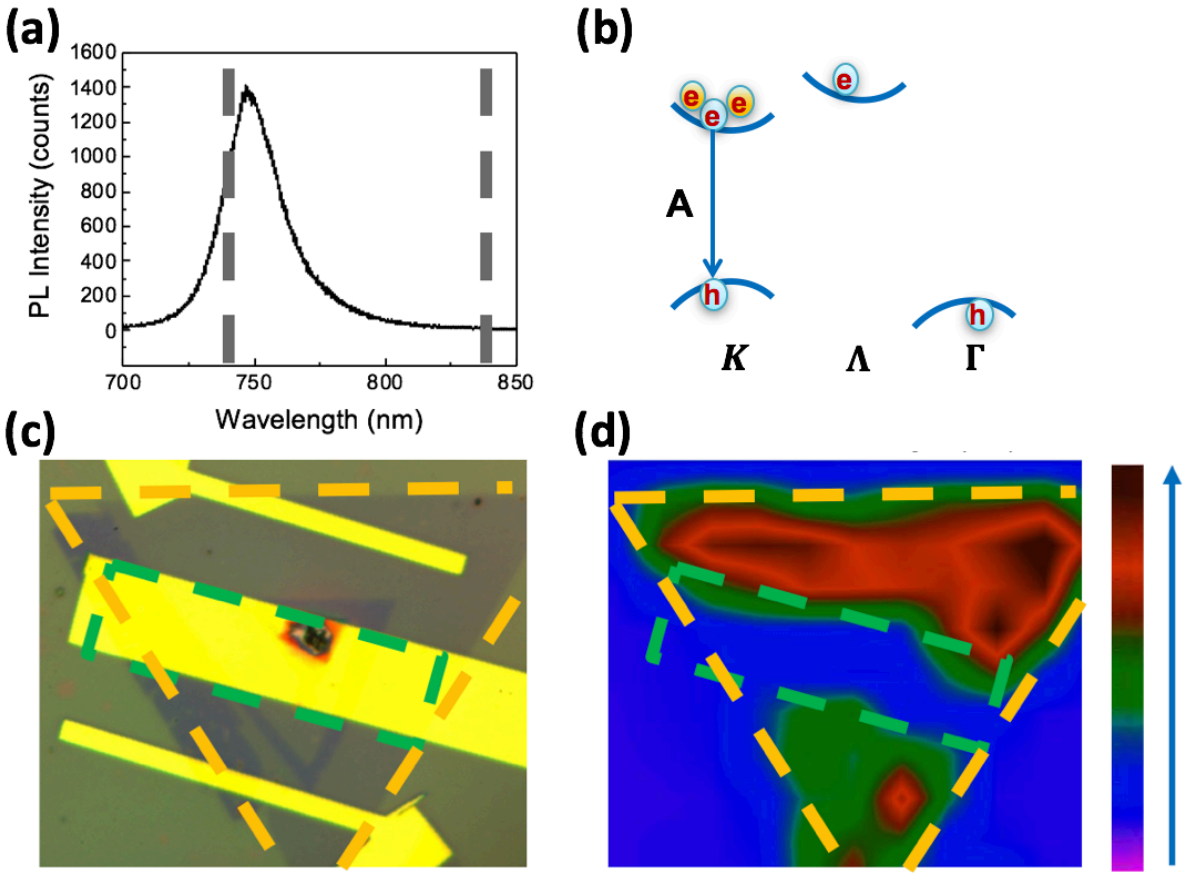


**Figure 2.18** (a) Photoluminescence spectrum of as-grown monolayer $WSe_2$. The grey dash lines indicate the range of the mapping. (b) Illustration of band structure of monolayer $WSe_2$, the arrow indicates the direct band transition A (K→K), yellow electron symbols indicate the hot electron. (c) Optical image of transferred monolayer $WSe_2$ on thin gold bar substrate. (d) Photoluminescence mapping of (c), mapping range is the gray dash lines range (740 – 840 nm), the green dash line is the area of the thin gold bar, the yellow dash line is the area of the transferred monolayer $WSe_2$, the arrow next to the color bar indicates the count increase direction of the color bar.

## 2.4 Conclusion

In the few-layer $WSe_2$ and gold thin film model system, we observed extra photoluminescence peak emergence when compared to the few-layer $WSe_2$ on the $SiO_2$/Si substrate. Based on the possible electron transitions of the few-layer $WSe_2$, we made an assumption that this phenomenon was related to the hot electron transfer process. We did control experiments to confirm that the newly emergence photoluminescence peak was originated from the hot electron transfer process. The different stacking angle experiment proved that the observed spectrum of the model system consisted of three transitions, they are possible transitions for few-layer $WSe_2$, A ($K \rightarrow K$) direct transition, $I_1$ ($K \rightarrow \Gamma$) indirect transition and $I_2$ ($\Lambda \rightarrow \Gamma$) indirect transition.

With the relationship of photoluminescence peak and hot electron injection, we used few-layer $WSe_2$ as a “probe” to study the hot electron injection mechanism. We changed the hot electron amount by changing the injection laser intensity, and we found out that the hot electrons would inject into both the $K$ valley and the $\Lambda$ valley, leading to the increased photoluminescence intensity of A ($K \rightarrow K$) direct transition and $I_2$ ($\Lambda \rightarrow \Gamma$) transition indirect transition. The transition pathway was determined by the possible transition pathways of the few-layer $WSe_2$.

With more of hot electrons injected, they tended to inject into the $K$ valley of the few-layer $WSe_2$, and photoluminescence intensity of $I_1$ ($K \rightarrow \Gamma$) indirect transition increased, leading to the shift of the peak, which was the combination of A ($K \rightarrow K$) and $I_1$ ($K \rightarrow \Gamma$) transition photoluminescence peak. The hot electron relaxation preferred pathways with lower energy difference.

At the last section, we compared the spectra of the model system with few-layer $WSe_2$ and that with monolayer $WSe_2$, and the results showed that the injection efficiency was related to the valley level. Monolayer didn’t have valley with level lower than that of $K$ valley, the hot electron injection efficiency was low and even led to photoluminescence quench which was electron back-

transfer to the gold film. With this finding, we could provide further explanation for the photoluminescence peak evolution with different laser intensity, that is, with more hot electrons injected into the few-layer $WSe_2$ the hot electrons would inject into the Λ valley and when it reached "saturation", hot electrons would "overflow" to K valley, as showed in Figure 2.18.

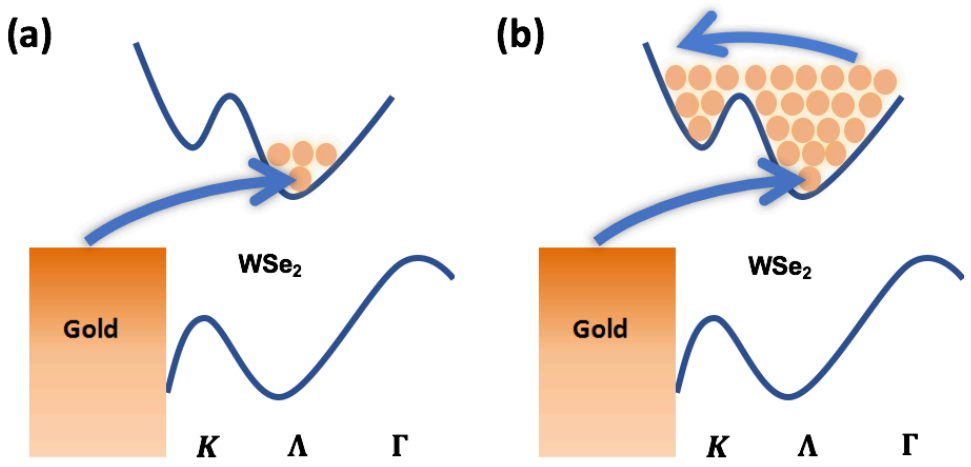


**Figure 2.19** (a) Schematic illustration of low hot electron injection. (b) Schematic illustration of large hot electron injection. The arrows indicate the hot electron injection direction.

### 2.5 References


1. Mubeen, S., Lee, J., Singh, N., Krämer, S., Stucky, G. D., & Moskovits, M. (2013). An autonomous photosynthetic device in which all charge carriers derive from surface plasmons. *Nature Nanotechnology*, *8*(4), 247-251.
2. Lee, S. W., Hong, J. W., Lee, H., Wi, D. H., Kim, S. M., Han, S. W., & Park, J. Y. (2018). The surface plasmon-induced hot carrier effect on the catalytic activity of CO oxidation on a Cu2O/hexoctahedral Au inverse catalyst. *Nanoscale*, *10*(23), 10835-10843.

3. Furube, A., Du, L., Hara, K., Katoh, R., & Tachiya, M. (2007). Ultrafast Plasmon-Induced Electron Transfer from Gold Nanodots into TiO2 Nanoparticles. *Journal of the American Chemical Society*, *129*(48), 14852-14853.
4. Shi, Y., Wang, J., Wang, C., Zhai, T., Bao, W., Xu, J., Xia, X., Chen, H. (2015). Hot Electron of Au Nanorods Activates the Electrocatalysis of Hydrogen Evolution on MoS2 Nanosheets. *Journal of the American Chemical Society*, *137*(23), 7365-7370.
5. Okuhata, T., Katayama, T., & Tamai, N. (2019). Ultrafast and Hot Electron Transfer in CdSe QD–Au Hybrid Nanostructures. *The Journal of Physical Chemistry C*, *124*(1), 1099-1107.
6. Ruan, D., Xue, J., Fujitsuka, M., & Majima, T. (2019). Ultrafast spectroscopic study of plasmon-induced hot electron transfer under NIR excitation in Au triangular nanoprism/g-C3N4 for photocatalytic H2 production. *Chemical Communications*, *55*(43), 6014-6017.
7. Cheng, J., Li, Y., Plissonneau, M., Li, J., Li, J., Chen, R., Tang, Z., Pautrot-d'Alençon, L., He, T., Tréguer-Delapierre, M., Delville, M. (2018). Plasmon-induced hot electron transfer in AgNW@TiO2@AuNPs nanostructures. *Scientific Reports*, *8*(1).
8. Yu, Y., Ji, Z., Zu, S., Du, B., Kang, Y., Li, Z., Zhou, Z., Shi, K., Fang, Z. (2016). Electron Transfer: Ultrafast Plasmonic Hot Electron Transfer in Au Nanoantenna/MoS2 Heterostructures. *Advanced Functional Materials*, *26*(35), 6393-6393.
9. Kim, H., Ahn, G. H., Cho, J., Amani, M., Mastandrea, J. P., Groschner, C. K., Lien, D. H., Zhao, Y., Ager, J. W., Scott, M. C., Chrzan, D. C., Javey, A. (2019). Synthetic WSe2 monolayers with high photoluminescence quantum yield. *Science Advances*, *5*(1), eaau4728.
10. Wang, Z., Dong, Z., Gu, Y., Chang, Y., Zhang, L., Li, L., Zhao, W., Eda, G., Zhang, W., Grinblat, G., Maier, S. A., Yang, J. K. W., Qiu, C., Wee, A. T. (2016). Giant photoluminescence enhancement in tungsten-diselenide–gold plasmonic hybrid structures. *Nature Communications*, *7*(1).

11. Pradhan, N. R., Garcia, C., Holleman, J., Rhodes, D., Parker, C., Talapatra, S., Terrones, M., Balicas, L., McGill, S. A. (2016). Photoconductivity of few-layered p-WSe2 phototransistors via multi-terminal measurements. *2D Materials*, *3*(4), 041004.
12. Jin, X., Li, Q., Li, Y., Chen, Z., Wei, T., He, X., & Sun, W. (2014). Energy level control: toward an efficient hot electron transport. *Scientific Reports*, *4*(1).
13. Yin, J., Li, J., Chen, H., Wang, J., Yan, P., Liu, M., Liu, W., Lu, W., Xu, Z., Zhang, W., Wang, J., Sun, Z., Ruan, S. (2017). Large-area highly crystalline WSe2 atomic layers for ultrafast pulsed lasers. *Optics Express*, *25*(24), 30020.
14. Han, A., Aljarb, A., Liu, S., Li, P., Ma, C., Xue, F., Lopatin, S., Yang, C., Huang, J., Wan, Y., Zhang, X., Xiong, Q., Huang, K., Tung, V., Anthopoulos, T. D., Li, L. (2019). Growth of 2H stacked WSe2 bilayers on sapphire. *Nanoscale Horizons*, *4*(6), 1434-1442.
15. Lee, H. S., Kim, M. S., Kim, H., & Lee, Y. H. (2016). Identifying multiexcitons in MoS2 monolayers at room temperature. *Physical Review B*, *93*(14).
16. Mak, K. F., He, K., Lee, C., Lee, G. H., Hone, J., Heinz, T. F., & Shan, J. (2012). Tightly bound trions in monolayer MoS2. *Nature Materials*, *12*(3), 207-211.
17. You, Y., Zhang, X., Berkelbach, T. C., Hybertsen, M. S., Reichman, D. R., & Heinz, T. F. (2015). Observation of biexcitons in monolayer WSe2. *Nature Physics*, *11*(6), 477-481.
18. Lyons, T. P., Dufferwiel, S., Brooks, M., Withers, F., Taniguchi, T., Watanabe, K., Novoselov, K. S., Burkard, G., Tartakovskii, A. I. (2019). The valley Zeeman effect in inter- and intra-valley trions in monolayer WSe2. *Nature Communications*, *10*(1).
19. Liu, E., Van Baren, J., Lu, Z., Altaiary, M. M., Taniguchi, T., Watanabe, K., Smirnov, D., Lui, C. H. (2019). Gate Tunable Dark Trions in Monolayer WSe2. *Physical Review Letters*, *123*(2).
20. Barbone, M., Montblanch, A. R., Kara, D. M., Palacios-Berraquero, C., Cadore, A. R., De Fazio, D., Pingault, B., Mostaani, E., Li, H., Wantanabe, K., Taniguchi, T., Tongay, S., Wang

G., Ferrari, A. C., Atatüre, M. (2018). Charge-tuneable biexciton complexes in monolayer WSe2. *Nature Communications*, *9*(1).

21. Ye, Z., Waldecker, L., Ma, E. Y., Rhodes, D., Antony, A., Kim, B., Zhang, X., Deng, M., Jiang, Y., Smirnov, D., Watanabe, K., Taniguchi, T, Hong, J., Heinz, T. F. (2018). Efficient generation of neutral and charged biexcitons in encapsulated WSe2 monolayers. *Nature Communications*, *9*(1).
22. Zhang, M., Fu, J., Dias, A. C., & Qu, F. (2018). Optically dark excitonic states mediated exciton and biexciton valley dynamics in monolayer WSe2. *Journal of Physics: Condensed Matter*, *30*(26), 265502.
23. Zhao, W., Ribeiro, R. M., Toh, M., Carvalho, A., Kloc, C., Castro Neto, A. H., & Eda, G. (2013). Origin of Indirect Optical Transitions in Few-Layer MoS2, WS2, and WSe2. *Nano Letters*, *13*(11), 5627-5634.
24. Zhou, H., Wang, C., Shaw, J. C., Cheng, R., Chen, Y., Huang, X., Liu, Y., Weiss, N., Lin, Z., Huang, Y., Duan, X. (2014). Large Area Growth and Electrical Properties of p-Type WSe2 Atomic Layers. *Nano Letters*, *15*(1), 709-713.
25. Li, Z., Wang, T., Lu, Z., Jin, C., Chen, Y., Meng, Y., Lian, Z., Taniguchi, T., Watanabe, K., Zhang, S., Smirnov, D., Shi, S. (2018). Revealing the biexciton and trion-exciton complexes in BN encapsulated WSe2. Nature Communications, 9(1).
26. Voß, D., Krüger, P., Mazur, A., & Pollmann, J. (1999). Atomic and electronic structure of WSe2 from ab initiotheory: Bulk crystal and thin film systems. *Physical Review B*, *60*(20), 14311-14317.
27. Liu, B., Fathi, M., Chen, L., Abbas, A., Ma, Y., & Zhou, C. (2015). Chemical Vapor Deposition Growth of Monolayer WSe2 with Tunable Device Characteristics and Growth Mechanism Study. *ACS Nano*, *9*(6), 6119-6127.

28. Wang, S., Rong, Y., Fan, Y., Pacios, M., Bhaskaran, H., He, K., & Warner, J. H. (2014). Shape Evolution of Monolayer MoS2 Crystals Grown by Chemical Vapor Deposition. *Chemistry of Materials*, *26*(22), 6371-6379.
29. Chen, S., Gao, J., Srinivasan, B. M., Zhang, G., Sorkin, V., Hariharaputran, R., & Zhang, Y. (2019). Origin of ultrafast growth of monolayer WSe2 via chemical vapor deposition. *npj Computational Materials*, *5*(1).
30. Da Silva, A. C., Caturello, N. A., Besse, R., Lima, M. P., & Da Silva, J. L. (2019). Edge, size, and shape effects on WS2, WSe2, and WTe2 nanoflake stability: design principles from an ab initio investigation. *Physical Chemistry Chemical Physics*, *21*(41), 23076-23084.
31. Addou, R., Smyth, C. M., Noh, J., Lin, Y., Pan, Y., Eichfeld, S. M., Fölsch, S., Robinson, J. A., Cho, K., Feenstra, R. M., Wallace, R. M. (2018). One dimensional metallic edges in atomically thin WSe 2 induced by air exposure. *2D Materials*, *5*(2), 025017.
32. Yamamoto, M., Dutta, S., Aikawa, S., Nakaharai, S., Wakabayashi, K., Fuhrer, M. S., Ueno, K., Tsukagoshi, K. (2015). Self-Limiting Layer-by-Layer Oxidation of Atomically Thin WSe2. *Nano Letters*, *15*(3), 2067-2073.
33. Zhao, W., Ghorannevis, Z., Amara, K. K., Pang, J. R., Toh, M., Zhang, X., & Eda, G. (2013). Lattice dynamics in mono- and few-layer sheets of WS2 and WSe2. *Nanoscale*, *5*(20), 9677.
34. Del Corro, E., Terrones, H., Elias, A., Fantini, C., Feng, S., Nguyen, M. A., Mallouk, T. E., Terrones, M., Pimenta, M. A. (2014). Excited Excitonic States in 1L, 2L, 3L, and Bulk WSe2 Observed by Resonant Raman Spectroscopy. *ACS Nano*, *8*(9), 9629-9635.
35. Zhao, Y., Luo, X., Li, H., Zhang, J., Araujo, P. T., Gan, C. K., Wu, J., Zhang, H., Quek, S. Y. Dresselhaus, M. S., Xiong, Q. (2013). Interlayer Breathing and Shear Modes in Few-Trilayer MoS2 and WSe2. *Nano Letters*, *13*(3), 1007-1015.

36. Sahin, H., Tongay, S., Horzum, S., Fan, W., Zhou, J., Li, J., Wu, J., Peeters, F. M. (2013). Anomalous Raman spectra and thickness-dependent electronic properties of WSe2. *Physical Review B*, *87*(16).

37. Dadgar, A. M., Scullion, D., Kang, K., Esposito, D., Yang, E. H., Herman, I. P., Pimenta, M. A., Santos, E.-J. G., Pasupathy, A. N. (2018). Strain Engineering and Raman Spectroscopy of Monolayer Transition Metal Dichalcogenides. *Chemistry of Materials*, *30*(15), 5148-5155.

38. Courtade, E., Semina, M., Manca, M., Glazov, M. M., Robert, C., Cadiz, F., Wang, C. G., Taniguchi, T. Watanabe, K., Pierre, M., Escoffier, W., Ivchenko, E. L., Renucci, P., Marie, X., Amand, T., Urbaszek, B. (2017). Charged excitons in monolayer WSe2: Experiment and theory. *Physical Review B*, *96*(8).

39. Huang, S., Ling, X., Liang, L., Kong, J., Terrones, H., Meunier, V., & Dresselhaus, M. S. (2014). Probing the Interlayer Coupling of Twisted Bilayer MoS2 Using Photoluminescence Spectroscopy. *Nano Letters*, *14*(10), 5500-5508.

40. He, J., Hummer, K., & Franchini, C. (2014). Stacking effects on the electronic and optical properties of bilayer transition metal dichalcogenides MoS2, MoSe2, WS2, and WSe2. *Physical Review B*, *89*(7).

41. Xia, M., Li, B., Yin, K., Capellini, G., Niu, G., Gong, Y., Zhou W., Ajayan, P. M., Xie, Y. (2015). Spectroscopic Signatures of AA′ and AB Stacking of Chemical Vapor Deposited Bilayer MoS2. *ACS Nano*, *9*(12), 12246-12254.

42. Plechinger, G., Mooshammer, F., Castellanos-Gomez, A., Steele, G. A., Schüller, C., & Korn, T. (2015). Optical spectroscopy of interlayer coupling in artificially stacked MoS 2 layers. *2D Materials*, *2*(3), 034016.

43. Cao, B., & Li, T. (2014). Interlayer Electronic Coupling in Arbitrarily Stacked MoS2 Bilayers Controlled by Interlayer S–S Interaction. *The Journal of Physical Chemistry C*, *119*(2), 1247-1252.

44. Wang, Z., Chen, Q., & Wang, J. (2015). Electronic Structure of Twisted Bilayers of Graphene/MoS2 and MoS2/MoS2. *The Journal of Physical Chemistry C*, *119*(9), 4752-4758.

45. Van der Zande, A. M., Kunstmann, J., Chernikov, A., Chenet, D. A., You, Y., Zhang, X., Huang, P. Y., Berkelbach, T. C., Wang, L., Zhang, F., Hybertsen, M. S., Muller, D., Reichman, D. R., Heinz, T. F., Hone, J. C. (2014). Tailoring the Electronic Structure in Bilayer Molybdenum Disulfide via Interlayer Twist. *Nano Letters*, *14*(7), 3869-3875.

## Chapter 3 : Modulation of Hot Electron Transfer

### 3.1 Introduction

In Chapter 2, when talking about the experiment in the model system with monolayer $WSe_2$, we mentioned the electron back-transfer to the gold thin film. In this chapter, we are going to dig deeper into the hot electron relaxation pathways. Figure 3.1 showed the time scale of the plasmonic hot electron generation and transfer, although the hot electron back-transfer and chemical interface scattering have relatively higher timescale when compared to hot electron generation, it is still possible for these processes take place.[1-4] There are two possible relaxation pathways for the after the hot electron injected into the semiconductor (Figure 3.2). Our purpose for the study of hot electron transfer is to improve the hot electron collection, in Chapter 2, the hot electron injection mechanism gave us insights of increase hot electron injection efficiency, in this chapter, we are going to discuss modulation methods to improve the hot electron collection based on the possible injected hot electron relaxation pathways.

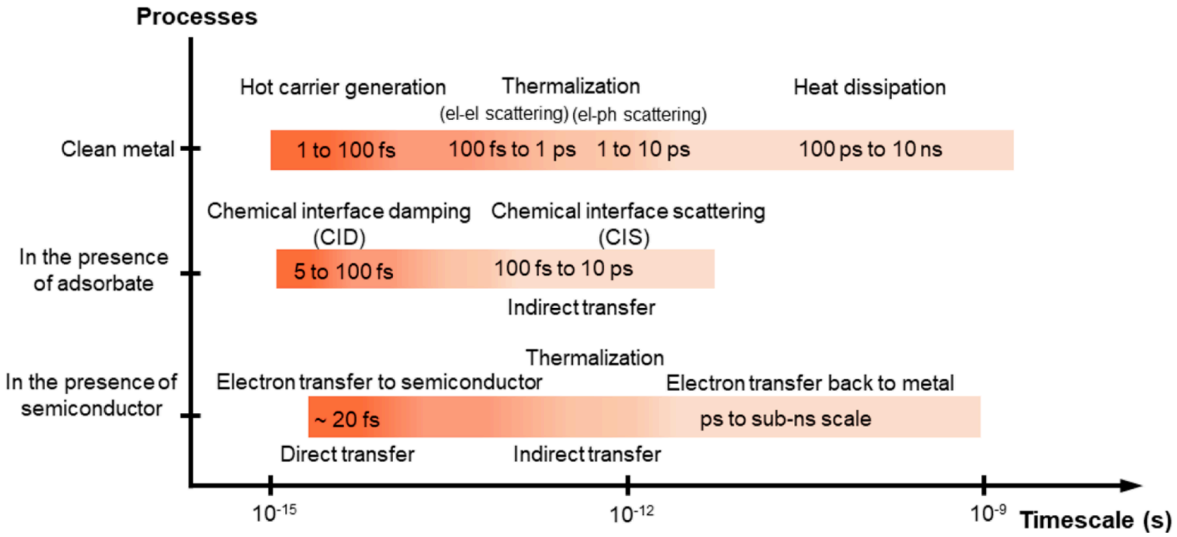


**Figure 3.1** Time scale of plasmonic hot electron generation and transfer in three different processes: clean metal, in the presence of adsorbate, in the presence of semiconductor.[1] Adapted with permission from Ref. 1. Copyright © 2018, American Chemical Society.

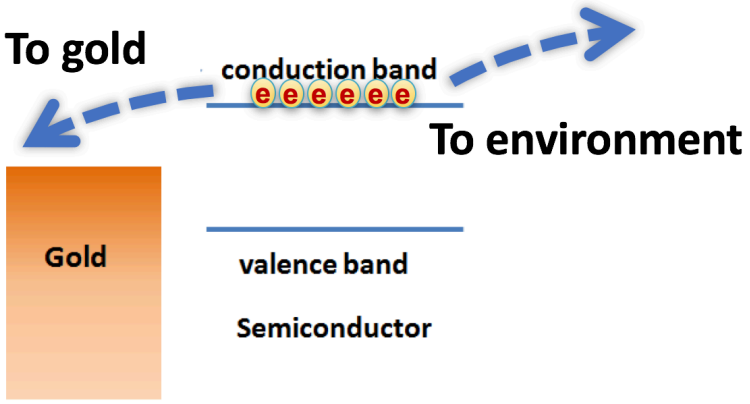


**Figure 3.2** Injected hot electron relaxation pathways. The dash arrows indicate the possible electron relaxation directions.

### 3.2 Design

We focus on the same model system, that is the few-layer $WSe_2$ transferred onto the gold thin film. There are two possible electron relaxation pathways, one is electron transfer to the environment, and the other one is transfer to the gold thin film (Figure 3.2). To prevent the hot electrons from relaxing into the environment or relaxing to the thin gold film. Here we put forward two schemes to tackle the two relaxation pathways mentioned above.

For the relaxation pathway from the few-layer $WSe_2$ to gold thin film, we designed an interlayer within the system to prevent to the hot electron from transferring to the gold thin film. In this experiment, we selected the SAM (Self-Assembled Monolayer) as the interlayer. To keep the system simple and easy to study, we used the SAM with simple molecules, here we chose the molecules 1-decanethiol (denoted by C10, length 10 Å) and 1-octadecanethiol (denoted by C18, length 20 Å) for the study. Both of the molecules have similar structures with a thiol group connecting at the one end of the carbon chain. The SAM is assembled by forming Au-S bond between the thiol group and the gold thin film.[5-8] The idea of using interlayer to block the electron

relaxation pathway between the few-layer $WSe_2$ and the gold thin film was based on the electron transport property of SAM mentioned in the literature.[9-13] Since the electron transport along the carbon chain of the alkane thiol was tunneling, which was the same as the electron transport of hot electron injection at the metal-semiconductor junction. [14-18] The addition of the interlayer would not affect the hot electron transfer mechanism between gold and the semiconductor. The rationale behind adding the interlayer between the few-layer $WSe_2$ and the gold thin film was that the electric field would build up on the plasmonic excited gold surface, and the forward electron transport (from the gold surface to the other end of the carbon chain) would be favored over backward electron transport (from the carbon chain to the gold surface).[19] For the relaxation pathway from the few-layer $WSe_2$ to the gold thin film, with the alkane thiol SAM assembled between the few-layer $WSe_2$ and the gold thin film, based on the electron transport mechanism mentioned in the literature, the interlayer should be able to block the hot electron from back-transferring to gold thin film (Figure 3.3).

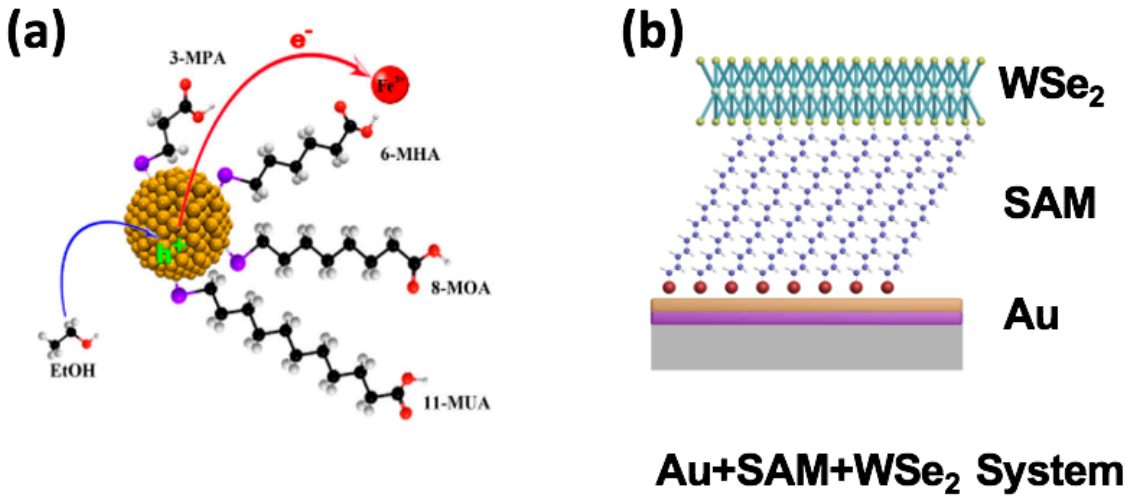


**Figure 3.3** (a) Illustration of hot electron transfer in alkane thiol SAM in the literature.[19] Adapted with permission from Ref. 19. Copyright © 2017, American Chemical Society. (b) Au-$WSe_2$ model system (transferred few-layer $WSe_2$ onto gold thin film) with SAM interlayer.

For another hot electron relaxation pathway from the few-layer $WSe_2$ to the environment, since we were using PMMA (Polymethyl methacrylate) in the wet transfer process to assist in transferring the as-grown few-layer $WSe_2$ to the gold thin film, to block this hot electron relaxation pathway we designed a simple way, that is, simply to leave the PMMA layer without dissolving it into the acetone. PMMA could stand temperature up to 200 $^{o}$C according to the thermal analysis and it also has high durability.[20-21] In the alloy industry, PMMA is often employed to resist corrosion.[22-25] In the chemistry, PMMA is widely used as protection layer due to its thermal and mechanical stability.[26-28] Hans-Joachim Egelhaaf *et al.* employed 65 nm PMMA to protect the conjugated polymer and effectively reduced the degradation rate.[29] Han Zhang *et al.* sandwiched the topological insulator between two layers of PMMA to fabricate the fiber laser that had high chemical stability.[30]

### 3.3 Experimental

#### 3.3.1 SAM Interlayer Experiments

To support the assumption that the addition of interlayer prevented the hot electrons from back-transferring to gold thin film, we took the photoluminescence spectra of the model system that is the stacking of gold thin film, alkane thiol SAM, few-layer $WSe_2$ on the $SiO_2$/Si substrate. The experimental process was listed as follows: (1) Deposited 40 nm gold thin film; (2) To assemble the SAM, the diluted solution with molecules was made, the concentration was 5 mM and the alcohol was used as the solvent. Then, the $SiO_2$/Si substrate with gold thin film was immersed into the solution overnight (about 12 h). After that, used a clean tweezer to carefully take out the substrate from the solution, and used isopropanol to triple rinse the sample (rinse the excess molecules to make sure monolayer was formed) and dried it with nitrogen; (3) Transferred the as-grown few-layer $WSe_2$ with the assistant of PMMA; (4) Took photoluminescence spectra of the sample.[31-35]

### 3.3.2 PMMA Protection Layer Experiments

To support the assumption that the PMMA layer could be used as the protection layer, the experiment and the related control experiments were designed as follows: (1) Transferred the as-grown few-layer $WSe_2$ onto the gold thin film with the assistant of PMMA and leave the PMMA without dissolving it; (2) Transferred the as-grown few-layer $WSe_2$ onto the gold thin film with the assistant of PMMA, and then immerse the sample into acetone for 15 min to dissolve the PMMA, followed by triple rinse with isopropanol and blow dry with nitrogen gun; (This step was to made the control sample) (3) Took the photoluminescence spectra of the samples made in step 1-3, and for the sample made in step 3, took the photoluminescence spectra both in the air (normal room environment) and in the vacuum. The vacuum environment was formed with a stainless steel chamber.

For all the spectra taken in the air, ND filter of 5% to adjust the laser intensity to 2 $\mu$W. For the spectra taken in the vacuum, we created the vacuum environment by putting the sample into a stainless still chamber which was connected to a pump, the chamber had a window made of quartz so that the laser could go through the window, and the photoluminescence could go through the window to the object lens to be collected by the spectrometer. Because of the chamber, the injected laser would be attenuated when the laser penetrated and reached the sample. Even though the window was made of quartz which had lower absortion than glass, it would still absorb a lot of injected laser, to take the spectrum of the sample in the vacuum, we used the largest ND filter 100% to use the highest possible intensity of the laser in our system. However, from the results we would discuess in the following section we could see that even we use the highest possible laser intensity in our systme, the photoluminescence intensity was still low, so during the comparison in the case of vacuum environment, we ignored the

photoluminescence counts and focused on the peak positions. Please note that the experiements we mentioned in the previous sections were performed with PMMA protection.

### 3.4 Results and Discussion

#### 3.4.1 SAM Interlayer Results and Discussion

Figure 3.4 compared the photoluminescence spectra of the samples with different carbon chain lengths. The photoluminescence spectra in the figure are of the same intensity scale. The photoluminescence spectra showed that carbon chain with different lengths led to different photoluminescence responses. Photoluminescence spectrum was closely related to the hot electrons and electron transfer process. The following section would discuss what was the impact to the hot electron injection with the addition of the SAM interlayer added into the system of gold thin film and few-layer $WSe_2$.

The photoluminescence intensity of model system with C18 SAM as the interlayer decreased, when compared to that of the model system without the SAM interlayer. We observed only one photoluminescence peak in the spectrum of model system with C18 SAM as the interlayer, and the peak was at 760 nm which corresponds to the $I_1$ ($K \rightarrow \Gamma$) indirect transition. And the spectrum was very similar to that of the as-grown few-layer $WSe_2$, which meant that the addition of an interlayer of about 20 Å blocked the hot electron transfer pathway from the gold thin film to few-layer $WSe_2$, making the photoluminescence spectrum similar to that of the as-grown few-layer $WSe_2$.

The photoluminescence intensity of model system with C10 SAM as the interlayer increased, when compared to that of the model system without the SAM interlayer. Unlike the photoluminescence spectrum of the system with the C18 SAM interlayer, the photoluminescence spectrum of the system with the C10 SAM interlayer showed two peaks. The photoluminescence spectrum of the system with the C10 SAM interlayer had the same pattern (including the peak

relative intensity as well as peak position) as the large hot electron injection situation mentioned in Section 2.3.3. In the spectrum, one of the peak was at 760 nm $I_1$ ($K \rightarrow \Gamma$) indirect transition and the other is at 830 nm $I_2$ ($\Lambda \rightarrow \Gamma$) indirect transition. This observation could support our assumption that due to the electron transport property of alkane thiol SAM, the addition of SAM with 10 Å carbon chain length as an interlayer to the system could effectively block the hot electron back-transfer pathway from the few-layer $WSe_2$ to the gold thin film. The length of the carbon chain of the SAM could not be too long, the length of 20 Å would lead to the blockage of hot electron injection.

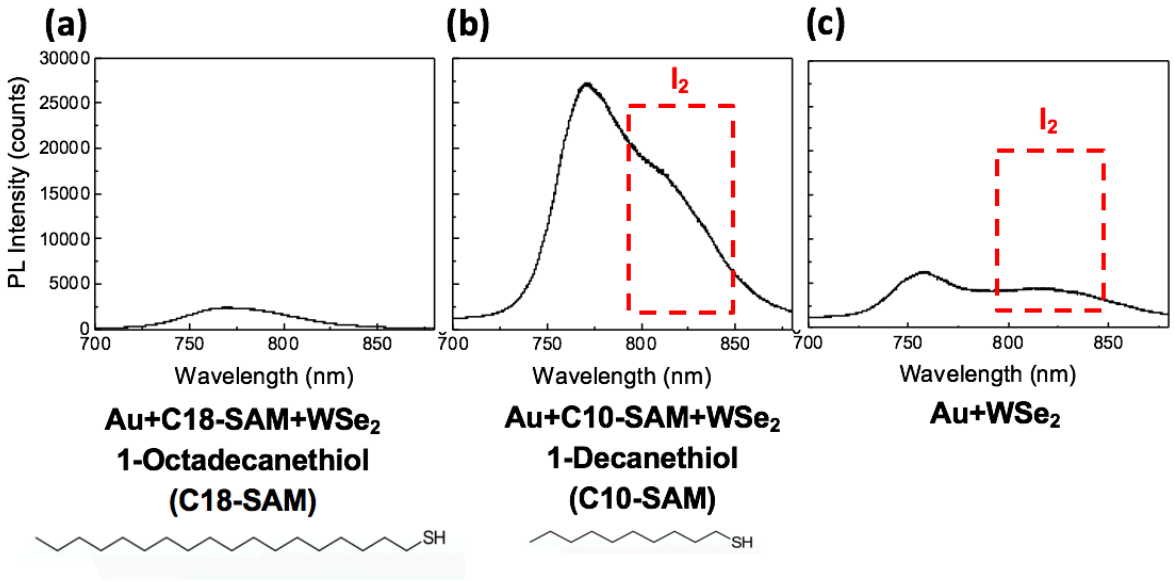


**Figure 3.4** Photoluminescence spectrum of the model system of gold thin film and few-layer $WSe_2$ with the addition of (a) 1-Octadecanethiol (C18 SAM) interlayer, (b) 1-Decanethiol (C10 SAM) interlayer, (c) no interlayer.

### 3.4.2 PMMA Protection Layer Results and Discussion

The results for the experiment to support the assumption that the PMMA could be the protection layer were showed in Figure 3.5. The when compared the spectrum of the samples with the PMMA protection and that of the samples without the PMMA protection, one photoluminescence peak was observed in the spectrum of the sample without PMMA protection, while two photoluminescence peaks were observed in the spectrum of the sample with PMMA protection. With respect to the intensity, higher photoluminescence intensity for the sample with PMMA protection were observed.

Figure 3.5 (b) showed the spectra of the samples without the PMMA protection, for the photoluminescence spectra of few-layer $WSe_2$ flake transferred on the $SiO_2$/Si substrate and on the gold thin film, only one photoluminescence peak was observed, the $I_2$ ($\Lambda \rightarrow \Gamma$) indirect transition could not be obaserved. Without the PMMA protection, for the sample transferred onto the thin gold film, the photoluminescence quenched (intensity lower) when compared to that of the sample on the $SiO_2$/Si substrate. This comparison indicated that the reason of the photoluminescence quench was the exposure to the air environement. For the transfer pathway, the hot electrons might transfer to the environment, also they might back-transfer to the gold thin film under the impact of the environment. From the electron transition timescale showed in Figure 3.1, the interaction with the adsorbates had shorter timescale, which meant that the hot electron in the few-layer $WSe_2$ had higher probability to interact with the molecules in the air than back-transfer to the gold thin film.

To provide further support to the assumption that the PMMA is the protection layer to prevent the hot electron from relaxing to the molecules in the environment, we placed the sample without the PMMA protection into a vacuum chamber. For the spectrum taken for the sample in the vacuum chamber, two photoluminescence peaks were observed, with one at 760 nm $I_1$ ($K \rightarrow \Gamma$) indirect transition, and the other at 830 nm $I_2$ ($\Lambda \rightarrow \Gamma$) indirect transition. The photoluminescence

spectrum pattern was similar to the high intensity laser injection in Chapter 3. The low photoluminescence intensity is attributed to the attenuation from the quartz window of the vacuum chamber. These experiment results confirm that the hot electrons are able to transfer to the air in the environment, and the PMMA protection could effectively block this relaxation pathway.

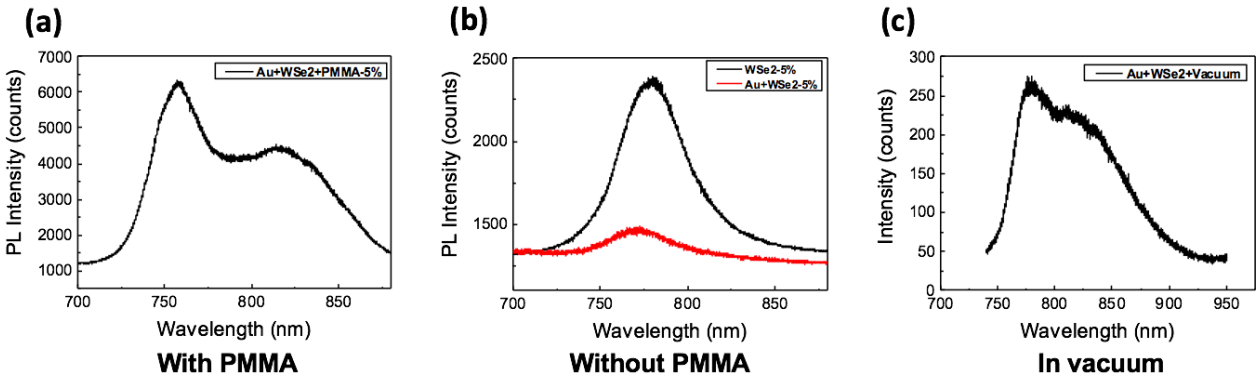


**Figure 3.5** (a) Photoluminescence spectrum of transferred few-layer $WSe_2$ onto gold thin film model system with PMMA protection layer. (b) Photoluminescence spectra of samples without PMMA protection layer. The black curve is the spectrum of the transferred few-layer $WSe_2$ onto $SiO_2$/Si substrate model system. The red curve is the spectrum of the transferred few-layer $WSe_2$ onto the gold thin film model system. (c) Photoluminescence spectrum of transferred few-layer $WSe_2$ onto gold thin film model system in vacuum.

### 3.5 Conclusion

We designed two modulation schemes based on the possible hot electron relaxation pathways. One scheme was to sandwich an alkane thiol SAM within the model system to prevent the hot electron from back-transferring to gold thin film. The other scheme was to use PMMA as the protection layer to prevent the hot electron from interacting with the ambient environment.

In the alkane thiol SAM modulation scheme, the modulation was related to the length of the carbon chain. If the length of the molecules was about 20 Å, the system behaved like a suspended few-layer $WSe_2$ system. If the length of the molecules was about 10 Å, with the addition of this molecule, the photoluminescence displayed $I_2$ ($\Lambda \rightarrow \Gamma$) indirect transition at 830 nm, and the photoluminescence intensity increased, and this photoluminescence spectrum had the same pattern as the that of large hot electron injection in Section 2.3.3. The alkane thiol SAM with the length of about 10 Å effectively increased the hot electron collection.

In the PMMA protection modulation scheme, the control experiments demonstrated protection with the PMMA layer. With the PMMA protection layer, hot electron injection to the $\Lambda$ valley leading the increased photoluminescence intensity in the $I_2$ ($\Lambda \rightarrow \Gamma$) indirect band was clearly observed, while the sample without PMMA protection layer showed photoluminescence quench.

### 3.6 References


1. Zhang, Y., He, S., Guo, W., Hu, Y., Huang, J., Mulcahy, J. R., & Wei, W. D. (2017). Surface-Plasmon-Driven Hot Electron Photochemistry. *Chemical Reviews*, *118*(6), 2927-2954.
2. Tan, S., Liu, L., Dai, Y., Ren, J., Zhao, J., & Petek, H. (2017). Ultrafast Plasmon-Enhanced Hot Electron Generation at Ag Nanocluster/Graphite Heterojunctions. *Journal of the American Chemical Society*, *139*(17), 6160-6168.
3. Razdolski, I., Chekhov, A. L., Stognij, A. I., & Stupakiewicz, A. (2019). Ultrafast transport and relaxation of hot plasmonic electrons in metal-dielectric heterostructures. *Physical Review B*, *100*(4).
4. Harutyunyan, H., Martinson, A. B., Rosenmann, D., Khorashad, L. K., Besteiro, L. V., Govorov, A. O., & Wiederrecht, G. P. (2015). Anomalous ultrafast dynamics of hot

plasmonic electrons in nanostructures with hot spots. *Nature Nanotechnology*, *10*(9), 770-774.

5. O'Dwyer, C., Gay, G., Viaris de Lesegno, B., & Weiner, J. (2004). The Nature of Alkanethiol Self-Assembled Monolayer Adsorption on Sputtered Gold Substrates. *Langmuir*, *20*(19), 8172-8182.
6. Vericat, C., Vela, M. E., & Salvarezza, R. C. (2005). Self-assembled monolayers of alkanethiols on Au(111): surface structures, defects and dynamics. *Physical Chemistry Chemical Physics*, *7*(18), 3258.
7. Xue, Y., Li, X., Li, H., & Zhang, W. (2014). Quantifying thiol–gold interactions towards the efficient strength control. *Nature Communications*, *5*(1).
8. Pensa, E., Cortés, E., Corthey, G., Carro, P., Vericat, C., Fonticelli, M. H., Benítez, G., Rubert, A. A., Salvarezza, R. C. (2012). The Chemistry of the Sulfur–Gold Interface: In Search of a Unified Model. *Accounts of Chemical Research*, *45*(8), 1183-1192.
9. Liu, B., Bard, A. J., Mirkin, M. V., & Creager, S. E. (2004). Electron Transfer at Self-Assembled Monolayers Measured by Scanning Electrochemical Microscopy. *Journal of the American Chemical Society*, *126*(5), 1485-1492.
10. Finklea, H. O., Yoon, K., Chamberlain, E., Allen, J., & Haddox, R. (2001). Effect of the Metal on Electron Transfer across Self-Assembled Monolayers. *The Journal of Physical Chemistry B*, *105*(15), 3088-3092.
11. Protsailo, L. V., & Fawcett, W. (2000). Studies of electron transfer through self-assembled monolayers using impedance spectroscopy. *Electrochimica Acta*, *45*(21), 3497-3505.
12. Fan, F. F., Yang, J., Cai, L., Price, D. W., Dirk, S. M., Kosynkin, D. V., Yao, Y., Rawlett, A. M., Tour, J. M. Bard, A. J. (2002). Charge Transport through Self-Assembled Monolayers of Compounds of Interest in Molecular Electronics. *Journal of the American Chemical Society*, *124*(19), 5550-5560.

13. Mervinetsky, E., Alshanski, I., Lenfant, S., Guerin, D., Medrano Sandonas, L., Dianat, A., Gutierrez, R., Cuniberti, G., Hurevich, M., Yitzchaik, S., Vuillaume, D. (2019). Electron Transport through Self-Assembled Monolayers of Tripeptides. *The Journal of Physical Chemistry C*, *123*(14), 9600-9608.
14. Du, B., Lin, L., Liu, W., Zu, S., Yu, Y., Li, Z., Kang, Y., Peng, H., Zhu, X., Fang, Z. (2017). Plasmonic hot electron tunneling photodetection in vertical Au-graphene hybrid nanostructures. *Laser & Photonics Reviews*, *11*(1), 1600148.
15. Shiraishi, Y., Yasumoto, N., Imai, J., Sakamoto, H., Tanaka, S., Ichikawa, S., Ohtani, B., Hirai, T. (2017). Quantum tunneling injection of hot electrons in Au/TiO2plasmonic photocatalysts. *Nanoscale*, *9*(24), 8349-8361.
16. Wang, P., Krasavin, A. V., Nasir, M. E., Dickson, W., & Zayats, A. V. (2017). Reactive tunnel junctions in electrically driven plasmonic nanorod metamaterials. *Nature Nanotechnology*, *13*(2), 159-164.
17. Lee, T., Wang, W., & Reed, M. A. (2003). Mechanism of Electron Conduction in Self-Assembled Alkanethiol Monolayer Devices. *Annals of the New York Academy of Sciences*, *1006*(1), 21-35.
18. Akkerman, H. B., Naber, R. C., Jongbloed, B., Van Hal, P. A., Blom, P. W., De Leeuw, D. M., & De Boer, B. (2007). Electron tunneling through alkanedithiol self-assembled monolayers in large-area molecular junctions. *Proceedings of the National Academy of Sciences*, *104*(27), 11161-11166.
19. Kim, Y., Wilson, A. J., & Jain, P. K. (2017). The Nature of Plasmonically Assisted Hot-Electron Transfer in a Donor–Bridge–Acceptor Complex. *ACS Catalysis*, *7*(7), 4360-4365.
20. Costache, M. C., Wang, D., Heidecker, M. J., Manias, E., & Wilkie, C. A. (2006). The thermal degradation of poly(methyl methacrylate) nanocomposites with montmorillonite, layered double hydroxides and carbon nanotubes. *Polymers for Advanced Technologies*, *17*(4), 272-280.

21. EL-Bashir, S., Althumairi, N., & Alzayed, N. (2017). Durability and Mechanical Performance of PMMA/Stone Sludge Nanocomposites for Acrylic Solid Surface Applications. *Polymers*, *9*(11), 604.
22. Jin, W., Hao, Q., Peng, X., & Chu, P. K. (2016). Enhanced corrosion resistance and biocompatibilty of PMMA-coated ZK60 magnesium alloy. *Materials Letters*, *173*, 178-181.
23. Harb, S. V., Trentin, A., De Souza, T. A., Magnani, M., Pulcinelli, S. H., Santilli, C. V., & Hammer, P. (2020). Effective corrosion protection by eco-friendly self-healing PMMA-cerium oxide coatings. *Chemical Engineering Journal*, *383*, 123219.
24. Muñoz, L., Tamayo, L., Gulppi, M., Rabagliati, F., Flores, M., Urzúa, M., Azócar, M., Zagal, J. H., Encinas, M., V., Zhou, X., Thompson, G. Páez, M. (2018). Surface Functionalization of an Aluminum Alloy to Generate an Antibiofilm Coating Based on Poly(Methyl Methacrylate) and Silver Nanoparticles. *Molecules*, *23*(11), 2747.
25. Trentin, A., Harb, S. V., Uvida, M. C., Pulcinelli, S. H., Santilli, C. V., Marcoen, K., Pletincx, S., Terryn, H., Hauffman, T., Hammer, P. (2019). Dual Role of Lithium on the Structure and Self-Healing Ability of PMMA-Silica Coatings on AA7075 Alloy. *ACS Applied Materials & Interfaces*, *11*(43), 40629-40641.
26. Thi, Q. H., Kim, H., Zhao, J., & Ly, T. H. (2018). Coating two-dimensional MoS2 with polymer creates a corrosive non-uniform interface. *npj 2D Materials and Applications*, *2*(1).
27. Kim, D. H., Choi, S., Cho, N. G., Chang, Y., Kim, H., Hong, J., & Kim, I. (2009). High Stability InGaZnO[sub 4] Thin-Film Transistors Using Sputter-Deposited PMMA Gate Insulators and PMMA Passivation Layers. *Electrochemical and Solid-State Letters*, *12*(8), H296.
28. Atik, M., Luna, F. P., Messaddeq, S. H., & Aegerter, M. A. (1997). Ormocer (ZrO2-PMMA) films for stainless steel corrosion protection. *Journal of Sol-Gel Science and Technology*, *8*(1-3), 517-522.

29. Früh, A., Egelhaaf, H., Hintz, H., Quinones, D., Brabec, C. J., Peisert, H., & Chassé, T. (2018). PMMA as an effective protection layer against the oxidation of P3HT and MDMO-PPV by ozone. *Journal of Materials Research*, *33*(13), 1891-1901.
30. Wang, Q., Chen, Y., Miao, L., Jiang, G., Chen, S., Liu, J., Fu, X., Zhao, C., Zhang, H. (2015). Wide spectral and wavelength-tunable dissipative soliton fiber laser with topological insulator nano-sheets self-assembly films sandwiched by PMMA polymer. *Optics Express*, *23*(6), 7681.
31. Poirier, G. E., & Tarlov, M. J. (1994). The c(4X2) Superlattice of n-Alkanethiol Monolayers Self-Assembled on Au(111). *Langmuir*, *10*(9), 2853-2856.
32. Jalal Uddin, M., Khalid Hossain, M., Hossain, M. I., Qarony, W., Tayyaba, S., Mia, M., Pervez, M. F., Hossen, S. (2017). Modeling of self-assembled monolayers (SAMs) of Octadecanethiol and Hexadecanethiol on gold (Au) and silver (Ag). *Results in Physics*, *7*, 2289-2295.
33. Jun, Y., Zhu, X., & Hsu, J. W. (2006). Formation of Alkanethiol and Alkanedithiol Monolayers on GaAs(001). *Langmuir*, *22*(8), 3627-3632.
34. Kutsenko, V. Y., Lopatina, Y. Y., Bossard-Giannesini, L., Marchenko, O. A., Pluchery, O., & Snegir, S. V. (2017). Alkylthiol self-assembled monolayers on Au(111) with tailored tail groups for attaching gold nanoparticles. *Nanotechnology*, *28*(23), 235603.
35. Kim, Y. T., & Bard, A. J. (1992). Imaging and etching of self-assembled n-octadecanethiol layers on gold with the scanning tunneling microscope. *Langmuir*, *8*(4), 1096-1102.

## Chapter 4 : Hot Electron Transfer in Model System of Gold and $WS_2$

### 4.1 Introduction

$WS_2$ and $WSe_2$ are Tungsten-based dichacogenides, and both have hexagonal crystal structure, and their monolayer consists of sandwiched composition of X-M-X (M and X denote transition metal and chalcogen atoms respectively).[1-2] Similar to $WSe_2$, $WS_2$ is an attractive material for optoelectronics with unique optical properties and high carrier mobility.[3] We extended our study to the same model system but replace the few-layer $WSe_2$ with few-layer $WS_2$.

The spectra from the literature demonstrate that there are two possible transitions for the few-layer $WS_2$, one is A ($K \rightarrow K$) direct transition, and the other one is $I_2$ ($\Lambda \rightarrow \Gamma$) indirect transition.[4-7] When we compared Figure 4.1 and Figure 2.3, we could see that the photoluminescence peak evolutions with temperature are different for few-layer $WS_2$ and few-layer $WSe_2$. Figure 4.2 summarize the band structures and possible transitions within $WS_2$ and $WSe_2$.[4] The reason choosing few-layer $WS_2$ instead of the other layered semiconductor to study is that the few-layer $WS_2$ has similar band structure as few-layer $WSe_2$, however, the photoluminescence properties of the few-layer $WS_2$ is different from that of the few-layer $WSe_2$, which makes it an interesting material for this extended study to provide more supportive evidence as to our findings in the previous chapters.[8]

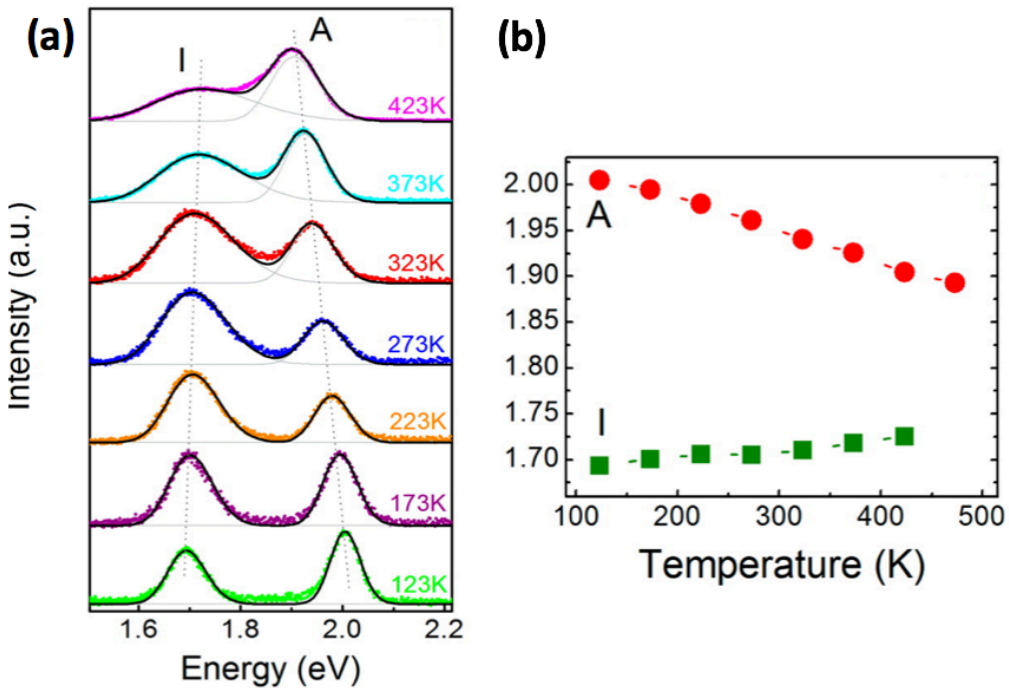


**Figure 4.1** (a) Photoluminescence spectra at different temperatures. (b) Photoluminescence peak positions as a function of temperature.[4]

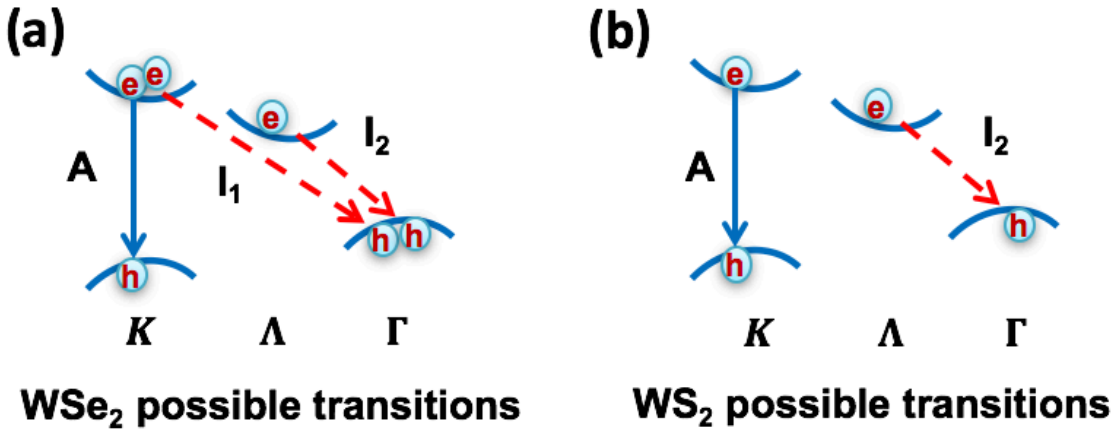


**Figure 4.2** Illustration of band structures of (a) $WSe_2$ and (b) $WS_2$, the arrows indicate the transition direction. Blue arrows indicate the direct transitions, red dash arrows indicate the indirect transitions.

### 4.2 Experimental

The layered material few-layer $WS_2$ fakes were synthesized with the CVD (chemical vapor deposition) method. The reaction took place in a quartz tube with 1-inch diameter in the 12-inch horizontal tube furnace (Lindberg Blue M) (Figure 4.3). 0.8 g $WS_2$ powder was placed onto the alumina combustion boat. A 2 x 2 cm 300 nm $SiO_2$/Si wafer with silicon oxide was placed at 5 cm away from the combustion boat at the gas down-stream side. The $WS_2$ powder boat was placed at the center of the hitting zone of the furnace. The furnace ramped up to 1100 $^oC$, and the growth would take place as it reached the melting point of the $WS_2$ powder. The argon gas was continuously supplied into the furnace at the flow of 50 sccm. After the growth last for 5 min, the growth was terminated by shutting off the furnace, and let it cool to room temperature naturally.[9] Figure 4.4 was the Raman spectrum of the as-grown $WS_2$. There were two vibration modes in the Raman spectrum, $E_{2g}$ in-plane mode at 354 $cm^{-1}$, and $A_{1g}$ out-of-plane mode at 419 $cm^{-1}$. In the literature, the monolayer $WS_2$ had the $E_{2g}$ peak was at 358 $cm^{-1}$ and $A_{1g}$ peak was at 419 $cm^{-1}$. From monolayer to few-layer, with the layer number increased, $E_{2g}$ softened due to the decreased Coulombic interaction between tungsten atoms.[10-18] We compared the Raman peak positions of the few-layer $WS_2$ with those of the monolayer $WS_2$ in the literature, we could confirm that the few-layer $WS_2$ was made.

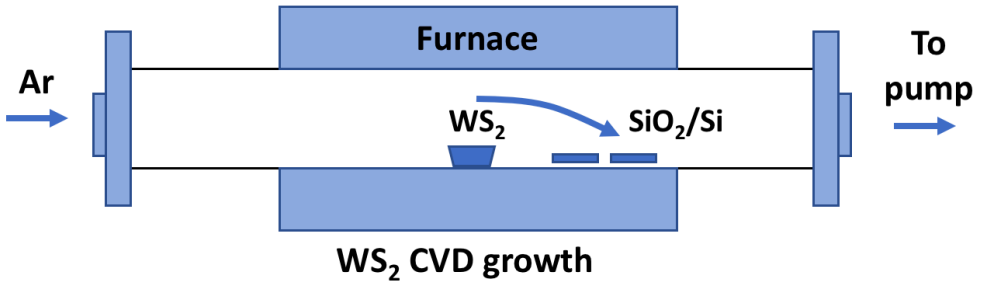


**Figure 4.3** Schematic illustration of the CVD furnace setup design for the growth $WS_2$ furnace. A 1-inch diameter quartz tube displays the relative locations of substrate and powder.

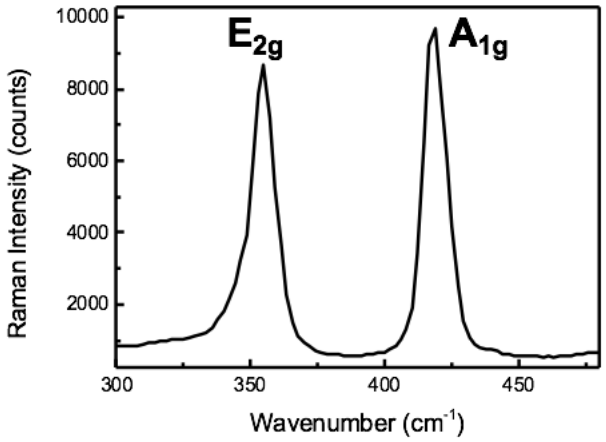


**Figure 4.4** Raman spectrum of the as-grown few-layer $WS_2$. The few-layer $WS_2$ had the $E_{2g}$ mode at 348 $cm^{-1}$, $A_{1g}$ mode at 412 $cm^{-1}$.

After the CVD process, the as-grown $WS_2$ was transferred to the gold thin film to made the gold - $WS_2$ model system for the study. The experimental process is listed as follows: (1) CVD grew the few-layer $WS_2$; (2) Deposited 40 nm thin gold film onto the 300 nm $SiO_2$/Si substrate; (3) Transferred the as-grown few-layer $WS_2$ onto the gold thin film with the assistant of PMMA and left the PMMA on the sample; (4) To make the control sample, repeat step 3, but the target substrate changed to the $SiO_2$/Si substrate without the gold thin film; (5) Took the photoluminescence spectra of the samples.

### 4.3 Results and Discussion

The model system was the same as that used Chapter 2 except that the few-layer $WSe_2$ was changed to few-layer $WS_2$. Figure 4.5 compared the spectra taken for as-grown $WS_2$ on the $SiO_2$/Si substrate and that of the as-grown $WS_2$ on the gold thin film. As expected, the spectra demonstrated the photoluminescence intensity increased of the indirect transition peak $I_2$ ($\Lambda \rightarrow \Gamma$). When compared to the spectrum of the few-layer $WSe_2$, in the spectrum of the few-layer $WS_2$, the

peak position of the first peak remained at the same position without shifting after the hot electron injection, while in the spectrum of the few-layer $WSe_2$ (Chapter 2), the peak position of the first peak redshifted to a higher wavelength, which was caused by the $I_1$ ($K \rightarrow \Gamma$) indirect transition. This results further confirmed that the hot electrons would inject into the lower $\Lambda$ valley of the few-layer $WS_2$, hot electron injection would increase the possibility of the indirect transition. And the hot electrons would also inject in the $K$ valley, leading to the increase in the possibility of A ($K \rightarrow K$) transition. The transitions were determined by all the possible transitions of the few-layer $WS_2$. Figure 4.1 and 4.2 showed that for few-layer $WS_2$ there were two possible transitions A ($K \rightarrow K$) and $I_2$ ($\Lambda \rightarrow \Gamma$), hot electron injection led to the increase of these two possible transitions, which meant that hot electron injection from the plasmonic surface to the 2D semiconductor would not change the band structure of the 2D semiconductor, it would only effect the transition rate of the possible transitions.

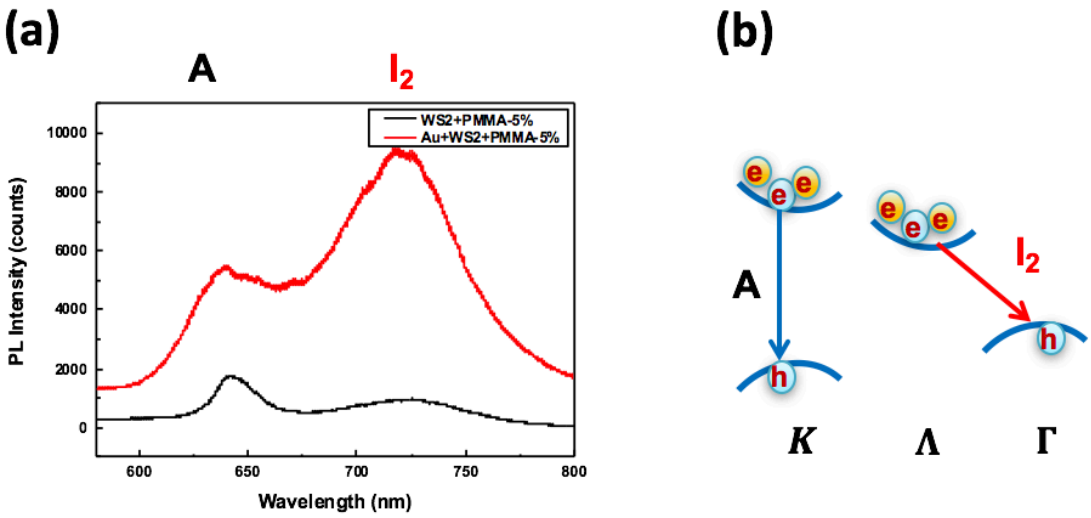


**Figure 4.5** (a) Photoluminescence of black curve few-layer $WS_2$ on the $SiO_2$/Si substrate, red curve few-layer $WS_2$ on the gold thin film. (b) Illustration of band structure and possible transitions

of few-layer $WS_2$, blue arrow denotes direct transition, red arrow denotes indirect transition. Yellow electron symbols denote injected hot electrons.

The as-grown few-layer $WS_2$ had two possible transitions, A ($K \rightarrow K$) and $I_2$ ($\Lambda \rightarrow \Gamma$) transition at different temperatures, unlike few-layer $WSe_2$, few-layer $WSe_2$ had $I_1$ ($K \rightarrow \Gamma$) indirect transition at room temperature but A ($K \rightarrow K$), $I_1$ ($K \rightarrow \Gamma$), and $I_2$ ($\Lambda \rightarrow \Gamma$) under different temperatures. Since few-layer $WS_2$ had not as rich photoluminescence peaks as few-layer $WSe_2$, few-layer $WS_2$ was not employed to study the hot electron transfer mechanism. From Figure 4.6 the laser intensity dependent photoluminescence spectra, we could employ the relative peak intensity difference from the A ($K \rightarrow K$) and $I_2$ ($\Lambda \rightarrow \Gamma$) transitions to further prove our assumption that hot electrons injected into the $\Lambda$ valley, leading to the increased indirect band transition photoluminescence. In Figure 4.6 (a), for the sample on the $SiO_2$/Si substrate, the pattern of the spectra remained the same with different laser intensities, the relative intensity of A ($K \rightarrow K$) and $I_2$ ($\Lambda \rightarrow \Gamma$) transitions remained the same. In Figure 4.6 (b), however, for the sample transferred on the gold thin film, a small injection 0.1% of the original laser intensity, relative more pronounced $I_2$ ($\Lambda \rightarrow \Gamma$) transition peak was observed. With the laser intensity increase, the relative intensity of the A ($K \rightarrow K$) transition also increased, this further proved our conclusion we made in the previous chapters that the hot electrons would tends to inject into the $\Lambda$ valley until it saturated and then injected into the $K$ valley.

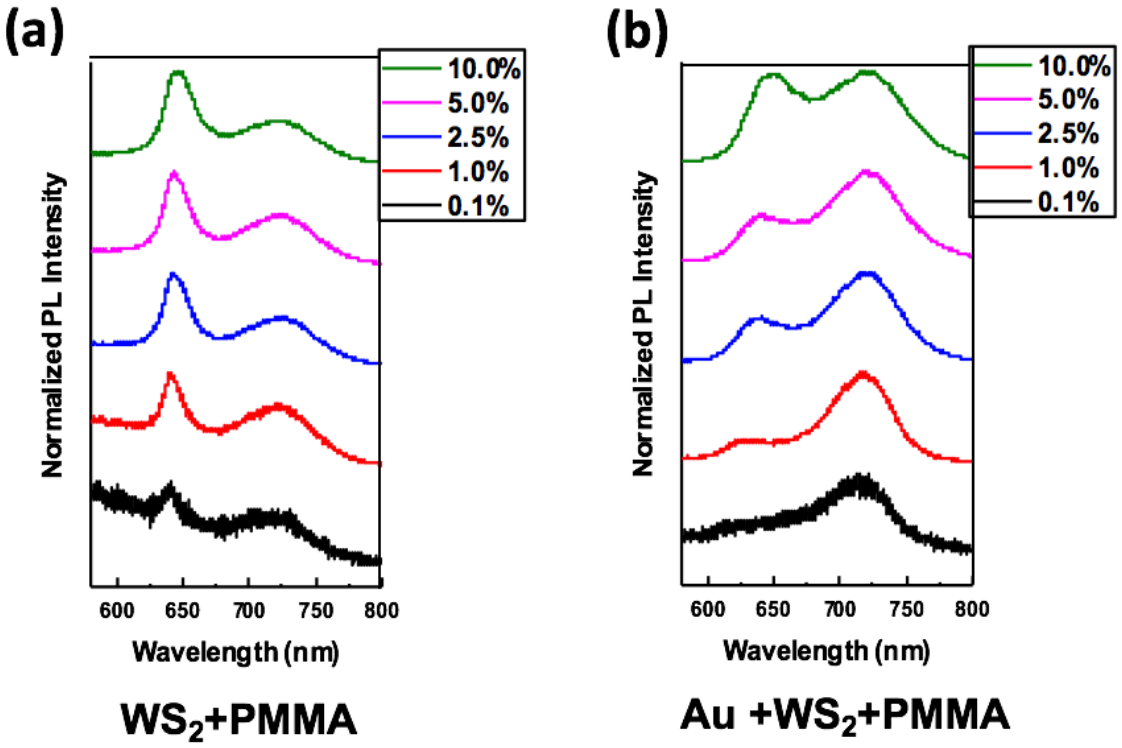


**Figure 4.6** (a) Photoluminescence spectra excited by different laser intensity, (a) few-layer $WS_2$ on the $SiO_2$/Si substrate, (b) few-layer $WS_2$ on the gold thin film.

### 4.4 Conclusion

We studied the model system with few-layer $WS_2$ and gold thin film. The few-layer $WS_2$ was employed in this extended study because few-layer $WS_2$ had similar chemical structure, band structure with few-layer $WSe_2$, but they have different transition pathways. With the hot electron injection mechanism put forward in the previous chapters, we were able to explain the observation in the model system with few-layer $WS_2$ and gold thin film. This experiment showed that hot electron injection was closely related to the band structure and possible transition pathways of the material. Hot electron tended to inject into the relatively lower valley $\Lambda$, and then injected into the relatively higher valley K. The study of the model system with few-layer $WS_2$ and gold thin film

provided further support for the hot electron injection mechanism we put forward in the previous chapter.

### 4.5 References


1. Rasmussen, F. A., & Thygesen, K. S. (2015). Computational 2D Materials Database: Electronic Structure of Transition-Metal Dichalcogenides and Oxides. *The Journal of Physical Chemistry C*, *119*(23), 13169-13183.
2. Eftekhari, A. (2017). Tungsten dichalcogenides (WS2, WSe2, and WTe2): materials chemistry and applications. *Journal of Materials Chemistry A*, *5*(35), 18299-18325
3. Huo, N., Yang, Y., & Li, J. (2017). Optoelectronics based on 2D TMDs and heterostructures. *Journal of Semiconductors*, *38*(3), 031002.
4. Zhao, W., Ribeiro, R. M., Toh, M., Carvalho, A., Kloc, C., Castro Neto, A. H., & Eda, G. (2013). Origin of Indirect Optical Transitions in Few-Layer MoS2, WS2, and WSe2. *Nano Letters*, *13*(11), 5627-5634.
5. Zhao, W., Ribeiro, R. M., Toh, M., Carvalho, A., Kloc, C., Castro Neto, A. H., & Eda, G. (2013). Origin of Indirect Optical Transitions in Few-Layer MoS2, WS2, and WSe2. *Nano Letters*, *13*(11), 5627-5634.
6. Ramasubramaniam, A., Naveh, D., & Towe, E. (2011). Tunable band gaps in bilayer transition-metal dichalcogenides. *Physical Review B*, *84*(20).
7. Li, W., Wang, T., Dai, X., Wang, X., Zhai, C., Ma, Y., & Chang, S. (2016). Bandgap engineering of different stacking WS2 bilayer under an external electric field. *Solid State Communications*, *225*, 32-37.
8. Dybała, F., Polak, M. P., Kopaczek, J., Scharoch, P., Wu, K., Tongay, S., & Kudrawiec, R. (2016). Pressure coefficients for direct optical transitions in MoS2, MoSe2, WS2, and WSe2 crystals and semiconductor to metal transitions. *Scientific Reports*, *6*(1).

9. Duan, X., Wang, C., Fan, Z., Hao, G., Kou, L., Halim, U., Li, H., Wu, X., Wang, Y., Jiang, J., Pan, A., Huang, Y., Yu, R., Duan, X. (2015). Synthesis of WS2xSe2–2x Alloy Nanosheets with Composition-Tunable Electronic Properties. *Nano Letters*, *16*(1), 264-269.
10. Elías, A. L., Perea-López, N., Castro-Beltrán, A., Berkdemir, A., Lv, R., Feng, S., Long, A. D., Hayashi, T., Kim, Y. A., Endo, M., Gutiérrez, H. R., Pradhan, N. R., Balicas, L., Mallouk, T. E., López-Urías, F., Terrones, H., Terrones, M. (2013). Controlled Synthesis and Transfer of Large-Area WS2 Sheets: From Single Layer to Few Layers. *ACS Nano*, *7*(6), 5235-5242.
11. Chakraborty, B., Matte, H. S., Sood, A. K., & Rao, C. N. (2012). Layer-dependent resonant Raman scattering of a few layer MoS2. *Journal of Raman Spectroscopy*, *44*(1), 92-96.
12. Berkdemir, A., Gutiérrez, H. R., Botello-Méndez, A. R., Perea-López, N., Elías, A. L., Chia, C., Wang, B., Crespi, V. H., López-Urías, F., Charlier, J., Terrones, H., Terrones, M. (2013). Identification of individual and few layers of WS2 using Raman Spectroscopy. *Scientific Reports*, *3*(1).
13. Li, Y., Li, X., Yu, T., Yang, G., Chen, H., Zhang, C., Feng, Q., Ma, J., Liu, W., Xu, H., Liu, Y., Liu, X. (2018). Accurate identification of layer number for few-layer WS2 and WSe2 via spectroscopic study. *Nanotechnology*, *29*(12), 124001.
14. Staiger, M., Gillen, R., Scheuschner, N., Ochedowski, O., Kampmann, F., Schleberger, M., … Maultzsch, J. (2015). Splitting of monolayer out-of-planeA1′Raman mode in few-layerWS2. *Physical Review B*, *91*(19).
15. Perea-López, N., Elías, A. L., Berkdemir, A., Castro-Beltran, A., Gutiérrez, H. R., Feng, S., Lv, R., Hayashi, T., López-Urías, F., Ghosh, S., Muchharla, B., Talapatra, S., Terrones, H., Terrones, M. (2013). Photosensor Device Based on Few-Layered WS2 Films. *Advanced Functional Materials*, *23*(44), 5511-5517.

16. Tan, H., Fan, Y., Zhou, Y., Chen, Q., Xu, W., & Warner, J. H. (2016). Ultrathin 2D Photodetectors Utilizing Chemical Vapor Deposition Grown WS2 With Graphene Electrodes. *ACS Nano*, *10*(8), 7866-7873.
17. Cunningham, P. D., McCreary, K. M., & Jonker, B. T. (2016). Auger Recombination in Chemical Vapor Deposition-Grown Monolayer WS2. *The Journal of Physical Chemistry Letters*, *7*(24), 5242-5246.
18. Yang, W., Shang, J., Wang, J., Shen, X., Cao, B., Peimyoo, N., Zou, C., Chen, Y., Wang, Y., Cong, C., Huang, W., Yu, T. (2016). Electrically Tunable Valley-Light Emitting Diode (vLED) Based on CVD-Grown Monolayer WS2. *Nano Letters*, *16*(3), 1560-1567.

**Chapter 5 : Conclusion**

Exploring the hot electron transfer mechanism between the plasmonic surface and the 2D semiconductor layered materials paves the way for the next generation photoelectrochemistry which is limited by the rapid relaxation of hot electrons before being transferred to the neighbor semiconductors.

In the first chapter, we discussed in detail about the generation and properties of the plasmonic hot electron in plasmonic nanostructure materials, we also talked about the properties of 2D semiconductor layered materials and the reason that we chose 2D semiconductor to study the hot electron transfer mechanism. At the end of this chapter we mentioned about the goal of this dissertation and the methods we employed for the mechanism study following chapters.

In the second chapter, we studied the model system of gold thin film and few-layer $WSe_2$, where few-layer $WSe_2$ was used as the probe to explore the hot electron injection mechanism between the gold thin film and the 2D semiconductor layered material. In this study, the photoluminescence spectrum was the used to assist in supporting the assumptions. The experiments demonstrated that hot electron injection was closely related to the band structure of the 2D semiconductor. For the few-layer $WSe_2$, the hot electron generated from the thin gold film would inject into the $\Lambda$ valley, leading to the increase in the possibility of the $I_2$ ($\Lambda \rightarrow \Gamma$) indirect transition. And with more hot electrons injected into the $\Lambda$ valley, the hot electrons would then inject into the $K$ valley, resulting in the increase of A ($K \rightarrow K$) direct transition and $I_1$ ($K \rightarrow \Gamma$) indirect transition. To further support the mechanism we put forward, we conducted stacking angle dependent photoluminescence, and also compared the spectra of the model system with few-layer $WSe_2$ and that of the model system with monolayer $WSe_2$.

In the third chapter, using the same model system with gold thin film and few-layer $WSe_2$, we investigated other possible hot electron relaxation pathways including the hot electron back transfer to gold thin film and the hot electron transfer to the environment. With the addition of the

alkane thiol SAM with appropriate carbon chain length as an interlayer in the system, the hot transfer back transfer to the gold thin film was effectively blocked, leading to the increase in the photoluminescence intensity. The addition of the PMMA protection layer in the system effectively protected the system from being affected by the environment which suppressed the quenching.

In the fourth chapter, we extended our experiment to the model system with few-layer $WS_2$, which having similar band structure as few-layer $WSe_2$ but different intrinsic transitions. With this few-layer $WS_2$ system, we repeated the experiments we did in the second chapter to provide further supports to the hot electron injection mechanism we put forward.